Development of a Data Acquisition System for the Air Shower Fluorescence Telescope FAMOUS

von

Julian Grothoff

Bachelorarbeit in Physik

vorgelegt der

Fakultät für Mathematik, Informatik und Naturwissenschaften der
Rheinisch-Westfälischen Technischen Hochschule Aachen

im August 2013

angefertigt am

III. Physikalischen Institut A

Abstract

FAMOUS[1] is a telescope prototype for the observation of fluorescence light produced by cosmic rays, based on Silicon Photomultipliers (SiPMs). As the prototype is ready for operation a Data Acquisition System(DAQ) is needed.

In this thesis a successfully build DAQ based on a Raspberry Pi mini computer combined with environment sensors connected to an Arduino microcontroller is introduced. A webinterface and the MongoDB database were installed. The webinterface can control the telescope prototype and has integrated run and calibration sequences. In the end a test measurement with minimum bias data was performed showing the stability of the temperature-adjusted voltage regulation and the quality of the calibration measurement for the breakdown-voltage of the SiPMs.

Auszug

FAMOUS[1] ist ein Teleskop prototyp basierend auf Silizium Photomultipliern(SiPMs) für die Beobachtung von Fluoreszenzlicht, welches von kosmischer Strahlung erzeugt wird. Da der Prototyp für den Betrieb bereit ist, wird ein Datenerfassungs System(DAQ) benötigt.

In dieser Arbeit wird ein erfolgreich erstelltes DAQ basierend auf einem Raspberry Pi mini Computer in Kombination mit Umwelt Sensoren, die mit einem Arduino Mikrocontroller verbunden sind vorgestellt. Darauf sind ein Webinterface und die MongoDB Datenbank installiert worden. Das Webinterface ist in der Lage den Teleskopprototypen zu steuern und hat integrierte Datenaufnahme und Kalibrations Mechanismen. Am Ende ist eine Testmessung mit wenigstens den Vorspannungsdaten gemacht worden, welche die Stabilität der Temperatur gesteuerten Spannungsregelung und die Qualität des Kalibrationsverfahrens für die Durchbruchspannung der SiPMs zeigt.

[1] First Auger Multi pixel photon counter camera for the Observation of Ultra-high-energy cosmic ray Showers

Erstgutachter

Prof. Dr. Thomas Hebbeker
III. Physikalisches Institut A
RWTH Aachen University

Zweitgutachter

Prof. Dr. Christopher Wiebusch
III. Physikalisches Institut B
RWTH Aachen University

Contents

1 Motivation

The discovery and research of cosmic rays has enriched mankind's knowledge in many ways. As technology improves, todays physicists are able to look deeper into our universe then ever before. To understand the sources and the character of high energy cosmic rays, the Pierre Auger Observatory was build in Argentina. Among other detector technologies the measurement of cosmic rays is achieved with highly sensitive fluorescence telescopes. To upgrade this already operating Fluorescence detector with Silicon Photon Multipliers the *First Auger Multi-pixel-photon-counter-camera for the Observation of Ultra-high-energy-cosmic-ray air Showers*(FAMOUS, cf. logo in figure 1.0.1) is developed at RWTH Aachen University.

A better understanding of cosmic rays and *ultra-high-energy cosmic rays* (UHECRs) in particular is essential for current astroparticle physics. These UHECRs are particles from outer space with energies above 1 EeV[1], which is "a hundred million times more energy than the particles produced in the world's most powerful particle accelerator"[1]. Joining high energy particle physics, astrophysics and cosmology many important questions are left open by UHECRs. These cosmic ray particles bombard the atmosphere of the Earth and produce an avalanche of secondary particles, referred to as *extensive air shower*. Furthermore, elastic collisions with nitrogen particles in the atmosphere produce fluorescence light all along their path to ground.

Pierre Victor Auger discovered that cosmic radiation events, respectively single particles are associated with extensive air showers [2] after Victor Hess found cosmic rays as an explanation for the radiation-levels in the atmosphere in 1912 .Whereas Pierre Auger researched in the mountains those days, the Pierre Auger Observatory, named after him, searches for highest energy particles in Argentina with a huge instrumented-area of about 3100 km^2. Basically a hybrid detector technique containing also 24 fluorescence telescopes is established . These telescopes use conventional *Photomultiplier Tubes* (PMTs) to measure the fluorescence photon flux.

FAMOUS is based on the promising new technology of *Silicon Photo-Multipliers* (SiPMs) as photon counters, with higher photon-detection-efficiencys compared to PMTs. The higher sensitivity to fluorescence light and the smaller dimensions of these chips will help to detect more distant and lower energy showers and thus lead to a deeper understanding of UHECRs. Up to now, many simulations for the construction of a prototype and characterization studies of possible SiPMs have been done [3] and a prototype with 7 pixels containing four SiPMs each, named $FAMOUS^7$ is operational at RWTH Aachen.

Before data of extensive air showers can be taken, the development of a *Data Aquisition System* (DAQ) is of great importance. Acquiring the data in automated runs ensures

[1] $1\ EeV = 10^{18}\ eV$

Figure 1.0.1: "First Auger Multi-pixel-photon-counter camera for the Observation of Ultra-high-energy cosmic ray Showers". The logo for FAMOUS.

data integrity and compatibility between measurements, especially for a later analysis. It prevents errors in data taking process by implementing tests and failsafe mechanisms as well. Moreover, the taken data can be stored in a database for easy, safe and fast access. Combined with a webserver, easy access of the collected Data, basic analysis and a device independent, worldwide control via network connection are possible applications. By the use of a *Raspberry Pi*[2] mini computer a small, low-cost server can be build. Connected to an *Arduino*[3] micro-controller board further run-time information during the measurements can be obtained by different environment sensors, which are collected in a database as well.

Outline The aim of this thesis is to develop and build a fully operational DAQ for FAMOUS with the Raspberry Pi, including an interface for recording sequences as control and an event display for these runs, and Arduino as environment sensor unit. The research of UHECRs with FAMOUS is introduced in chapter 2, explaining fluorescence detection of cosmic rays in general. After that, the development and the construction of the DAQ are documented concerning the requirements for this special purpose. Moreover, the used hardware and software components are introduced and noise measurements for the environment sensors are presented. Chapter 4 describes the implementation of a recording sequence for a run and how the taken data can be displayed. In addition a final test measurement with FAMOUS[7] is included. Closing in chapter 5, the effort of this work is evaluated and possible future improvements are specified.

[2]One-board credit-card-sized computer. See http://www.raspberrypi.org/faqs for details.
[3]Open-source electronics prototyping platform. See http://www.arduino.cc for details.

2 The Measurement of Cosmic Rays with FAMOUS

To observe the highest energy cosmic rays at the Pierre Auger Observatory with a multi-photon-pixel-counter-camera based on silicon photomultipliers FAMOUS is build at RWTH Aachen university. In this chapter basic information on cosmic rays especially is presented. Furthermore, extensive air showers are described and their observation by fluorescence technique is considered as well. After that, the baseline design for FAMOUS and the design of the Prototype FAMOUS[7] is characterised.

2.1 Ultra-High-Energy Cosmic Rays

The history of research for cosmic rays started early in 1912 [4] when Victor Hess found the increasing ionisation of the air with increasing altitude. He concluded that the source of the ionisation lies in outer-space and not in the radiation of radioactive material in the Earth as believed before. The first ghostly tracks left by cosmic rays were photographed by Dimitri Skobelzyn in 1927 [5]. Eleven years later, Pierre Auger measured coincident events in different particle detectors positioned in the alps several 10 meters apart from each other. P. Auger assumed that both events were secondary particles of an "extensive air shower" produced by a particle hitting the atmosphere of the Earth and hence calculated the energy of this cosmic ray to 10^{15} eV. Afterwards the first ultra-high-energy cosmic ray with an energy of 10^{20} eV was detected in 1962 by John Linsley and his collaborators at the Volcano Ranch experiment in New Mexico.

These high energetic charged particles from the cosmos, which are mostly protons or heavier nuclei like helium, nitrogen or even iron, hit the atmosphere of the Earth from diverse directions traveling with nearly the speed of light. Due to energies up to 10^{20} eV cosmic rays produce an avalanche of secondary particles after hitting a nucleus of a molecule in the air, referred to as extensive air shower. Cosmic rays have been measured over a huge energy range by various experiments. Their energy flux follows a steep power law continuously falling with the primary particle energy as shown in figure 2.1.1, so that one particle per century and square kilometer at energies above 100 EeV can be observed.

It is still unknown where and how the particles are accelerated [1]. Reflections of charged particles at moving magnetic fields in supernovae is one possible explanation for the acceleration of cosmic rays, found by Enrico Fermi in 1949 [7]. The search and reconstruction of the sources is very complex, because in contrast to photons these particles are charged and get deflected by magnetic fields in the interstellar or intergalactic medium on their way to the Earth. However, scientists of the Pierre Auger

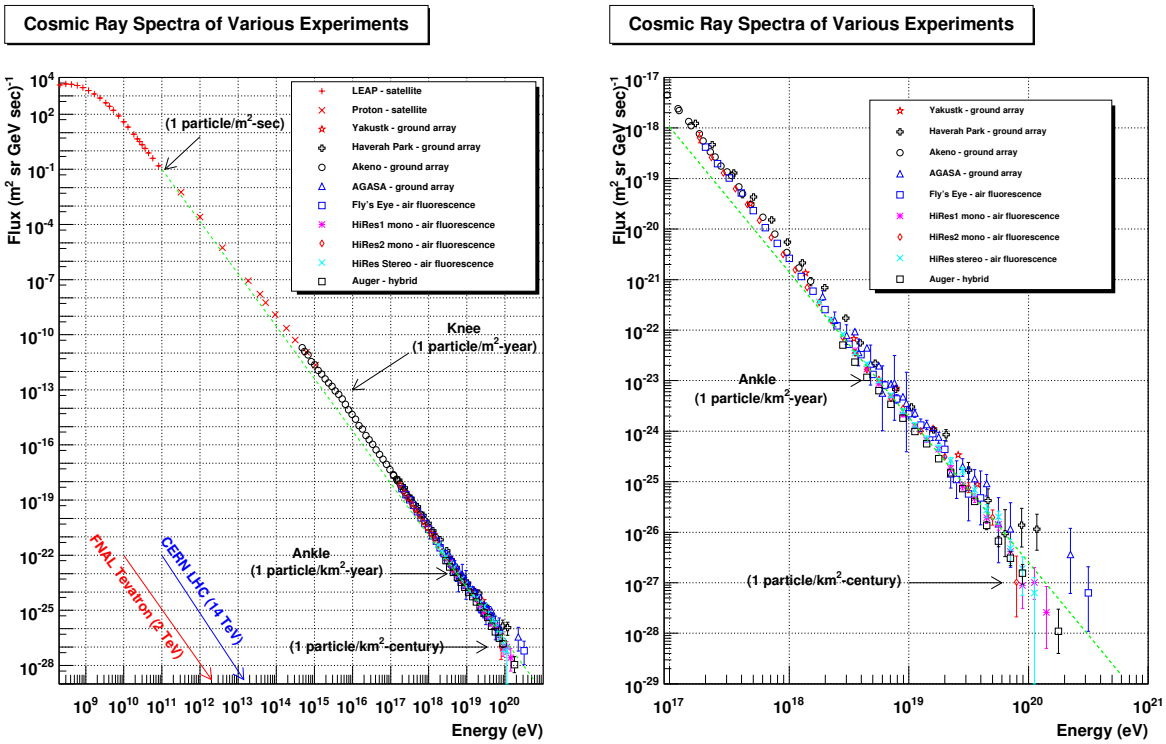

Figure 2.1.1: Flux of cosmic rays from extensive air shower measurements as function of the energy of the primary particle in two different energy ranges. The energy of the currently strongest accelerators and some exemplary fluxes are marked.[6]

Collaboration found out that possible sources of UHECRs could be Active Galactic Nuclei, probably containing super-massive black holes [8]. The sources should be close to our galaxy, because the highest energetic particles may interact with the microwave background reducing their energy while traveling through space. This would cut off the highest energetic particles from long distance in space, called the GZK-Cutoff proposed by Kenneth Greisen, Vadem Kuzmin and Georgi Zatsepin in 1966. Another possible thesis for the acceleration of the highest particles are collapsing relics left over from the Big Bang, called topological defects.

The essential questions for sources, acceleration mechanisms, energy-flux-dependence and chemical composition of UHECRs are still main part of ongoing research and the existing theories are waiting to be proofed. Due to this reason, the Pierre Auger project started in 1995 and marked its scientific launch in 2005 with the largest ground based detector on Earth. Thus, data collection, evaluation and improvements like FAMOUS will lead to an improved understanding of UHECRs.

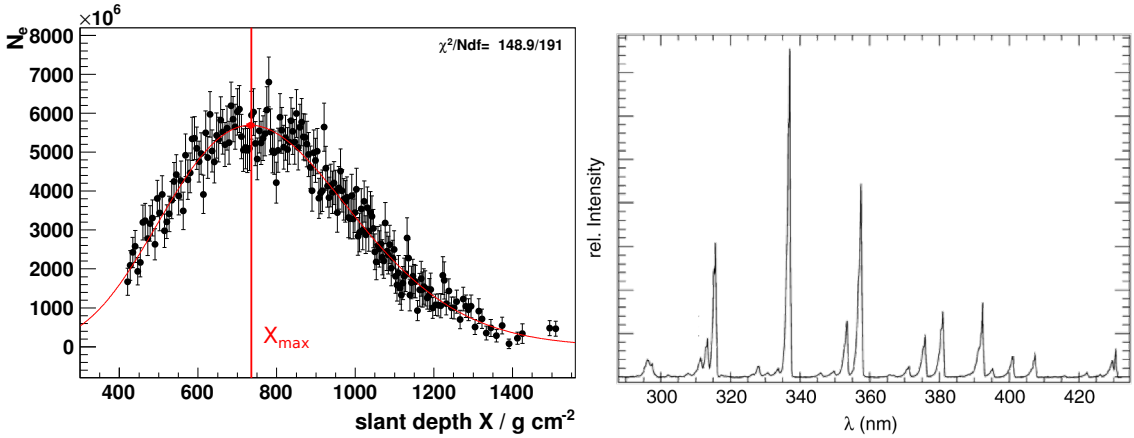

Figure 2.1.2: *Left:* Number of electrons and positrons N_e as function of the slant depth X. This event has been recorded by the Fluorescence Detector of the Pierre Auger Observatory at September 23, 2011 (event 12737439). The red line denotes the theoretical fit (Gaisser-Hillas-function). *Right:* Fluorescence light spectrum of air as measured with an electron beam of 3 MeV by AIRFLY experiment. The measurement was done at 20 °C and a pressure of 800 hPa [9].

2.2 The Fluorescence Detection Technique

2.2.1 Emission of Fluorescence Light

Extensive air showers basically consist of a muonic, hadronic and electromagnetic shower component. The shower particles excite nitrogen molecules, which consequently produce fluorescence light. To reconstruct the shower profile the energy deposit of electrons and positrons as shown in figure 2.1.2 has to be considered. After the first reaction with nuclei in the atmosphere happened, a shower of secondary particles is produced continuously. The number of particles rises until a maximum at a slant depth $X_{\max}$ and then the shower dies out. This contribution can be fitted by the Gaisser-Hillas-parametrisation [9] with the depth of the first interaction X_1 and the mean interaction length $\lambda_i nt$.

$$N_e(X) = N_{\max}\left(\frac{X - X_1}{X_{\max} - X_1}\right)^{\frac{X_{\max}-X_1}{\lambda_{\text{int}}}} \exp\left(\frac{X_{\max} - X_1}{\lambda_{\text{int}}}\right) \tag{2.2.1}$$

The number of produced fluorescence photons is proportional to the energy deposit E_{dep} via the light yield Y depending on the photon wavelength λ, the atmospheric pressure P, the ambient temperature T and the humidity u:

$$\frac{d^2N_\gamma}{dXd\lambda} = Y(\lambda, P, T, u) \cdot \frac{dE_{\text{dep}}}{dX} \propto \frac{dN_e}{dX}. \tag{2.2.2}$$

A typical light yield for UV fluorescence light is in the order of 5 $\text{MeV}^{-}1$.As the nitrogen molecules transit to their ground state from different electronic states in combination

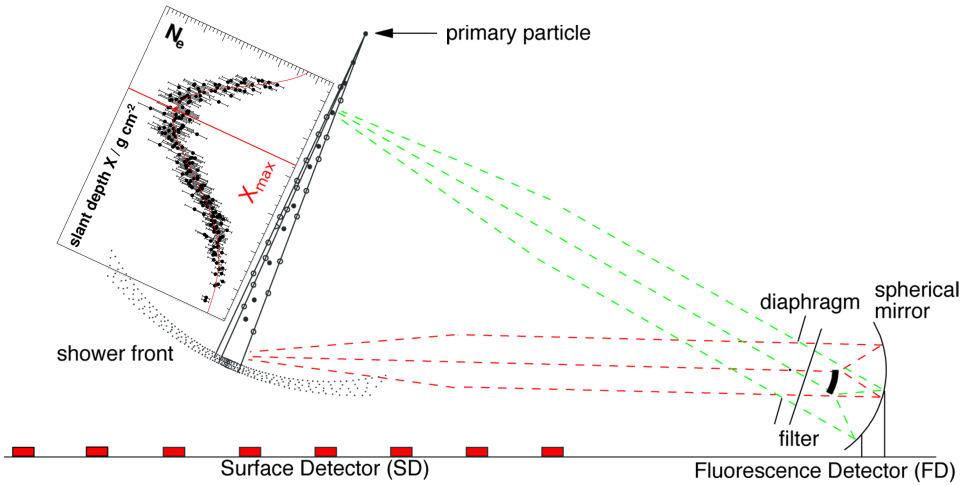

Figure 2.2.1: Working principle of a hybrid ground based fluorescence and surface detector as it is implemented at the Pierre Auger Observatory. Adapted from [10]. The typical longitudinal shower profile from above was integrated in the sketch.

with the change of the vibrational and rotational states ultraviolet (UV) light is emitted in range of about 300 nm to 400 nm as shown in the fluorescence spectrum in figure 2.1.2. Hence, the energy and direction of the primary particle can be determined by the longitudinal shower profile and the Gaisser-Hillas-shape.

2.2.2 Cosmic Ray Fluorescence Detection

At energies higher than 10^{16} eV, the UV signal is strong enough to measure the longitudinal profile of a shower by the fluorescence technique. A large ground-based detector is required to study cosmic rays at the highest energies, because of the very low particle flux, 1 particle per year and square-kilometer at 10^{18} eV for example (cf. figure 2.1.1). The working principle, as realised in the Pierre Auger Observatory, is shown figure 2.2.1. To calculate the energy distribution, the arrival time and an image of the light track have to be taken. So basically an image has to be formed on a camera consisting of a multi-pixel array in a telescope. So the precision of a measured light path depends on the resolution of the camera, the imaging properties and the PDE of the telescope. Moreover, a light track reconstructed from the observation of more than one telescope or a hybrid detection is much more accurate. This is because in a monocular observation the measured light path on the camera has to be used to construct a shower-plane and then only the pixel timing determines the position in that plane [9].

For a complete reconstruction, the fraction of Cherenkov light, which is a highly asymmetric background contribution, has to be estimated from the longitudinal shower profile. Furthermore, the wavelength depending atmospheric absorption of the emitted light, has to be determined. Thus a continuos observation of atmospheric conditions has to be done. Fluorescence light measurements can only be taken during moonless nights resulting in a lower duty-cycle of about 10 to 15 percent [11].

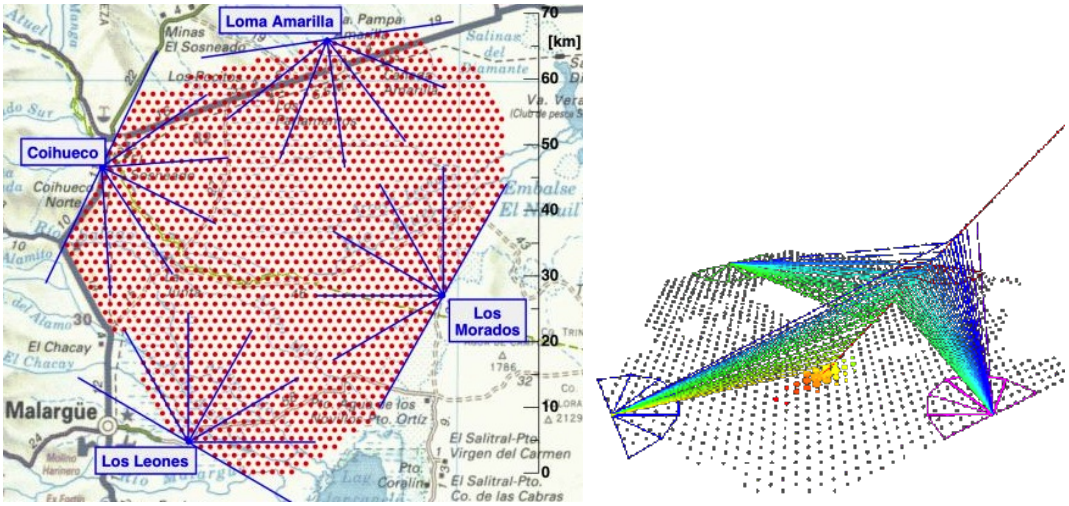

Figure 2.2.2: *Left:* Map of the Surface and Florescence Detectors in the southern site of the Auger Observatory in the "Pampa Amarilla" (yellow prairie) in western Argentina. *Right:* Reconstructed shower from Auger measurement seen by three of four telescope sites and the SD. The signal timing is color coded.

Besides Auger their were more smaller fluorescence detectors like Fly's Eye in Utah USA and its successor Fly's Eye II and HiRes I and II. Fly's Eye, which was the first of its kind operating for 10 years since 1982, detected the most energetic particle with an energy of $(3.2 \pm 0.9) \cdot 10^{20}$ eV. Other fluorescence detectors are the Telescope Array (TA), located in Millard County, Utah, USA and in the future the Auger north site with 18 planned telescopes in Colorado, USA with an even larger areal than the southern site [12].

2.2.3 Fluorescence Detector of the Pierre Auger Observatory

In the southern site of the Auger Observatory in Argentina basically an "hybrid detector" is established. To provide communication between each station and a central data acquisition system, a radio communication is installed (details in chapter 3). For the detection of charged particle footprints the *Surface Detector* array (SD) consists of over 1600 water-Cherenkov detectors, each containing 12 tons of water, instrumented by three 9" photomultipliers. As the world largest cosmic ray detector, covering approx 3000 km^2, the detectors are placed in a triangular grid of 1.5 km spacing. This whole area is overlooked by the *Fluorescence Detector* (FD) as shown in figure 2.2.2.

The hybrid detection technique plays a key role in the analysis of cosmic rays. A reconstruction of an extensive air shower seen by three telescopes is shown in figure 2.2.2. The FD at the Auger Observatory has four sites with six telescopes each.[1] The field of view of each telescope is 30° in azimuth, and 1.5° − 30° in elevation. Behind an UV-pass filter and a corrector ring a 12 m^2 big mirror is focussing light on a camera containing 440 hexagonal pixels, of 18 cm^2. The telescope construction constitutes a

[1] Not including different enhancements like HEAT.

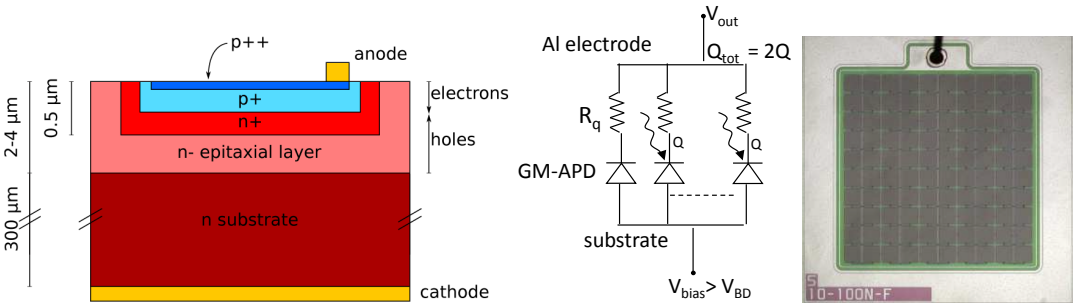

Figure 2.2.3: *Left*: Schematic of a Geiger-mode avalanche-photodiode without passivation layers and quenching resistors connected to the anode. Adapted from [13]. *Middle*: Equivalent circuit diagram for a SiPM [14]. *Right*: Close-up photo of a Hamamatsu Silicon-photomultiplier with 100 cells on 1 mm x 1 mm area [15].

modified Schmidt camera design that partially corrects spherical aberration and eliminates coma aberration. Every 0.1 μs a camera shot is taken. Each pixel consists of a light collector, a light funnel and a Photo-Multiplier-Tube (PMT). The used PMTs have a photocatode with a quantum efficiency of about 25 % in the UV range [11].

2.2.4 Silicon Photomultipliers

The usage of novel Silicon-Photo-Multipliers (SiPMs) instead of PMTs will improve the fluorescence detection. An SiPM is a semiconductor device containing an array of Geiger-mode *avalanche photodiodes* (APDs) referred to as cells. Thus another name for SiPMs as used in the acronym FAMOUS is "Multi-pixel-photon-counter". Due to collision ionisation during the avalanche breakdown the APDs amplify the signal of an electron-hole-pair produced by incoming photons with a gain similar to PMTs of approximately 10^6. Each cell in a SiPM is connected in series with a quenching resistor and all cells are placed on a common substrate in parallel connection (cf. left of figure 2.2.3). The combination of many binary cells produce an analog sum of all binary Geiger-mode APD signals. The number of triggered cells in one SiPM N_{trig} as function of the count of incoming photons N_λ derives from the number of cells N_{cell} and the Photo-detection-efficiency (PDE[2]):

$$N_{\text{trig}}(N_\lambda) = N_{\text{cells}}(1 - \exp(\{N_\lambda \frac{\text{PDE}(\lambda)}{N_{\text{cells}}}\}). \tag{2.2.3}$$

To operate the APD in Geiger-mode with a gain proportional to the over-voltage ($V_{OV} = V_{\text{bias}} - V_{\text{break}}$) the bias-voltage V_{bias} has to be calibrated depending on the cell breakdown-voltage V_{break} (for details see section 4.2). The PDE can also be increased by the use of higher over-voltages, but at the cost of increasing noise. Due to random thermal excitation, SiPMs show a thermal noise with a frequency in order of 1 kHz per cell at room temperature. The two observed correlated noise phenomena are

[2]The PDE combines the quantum efficiency with the geometric fill factor and the trigger probability.

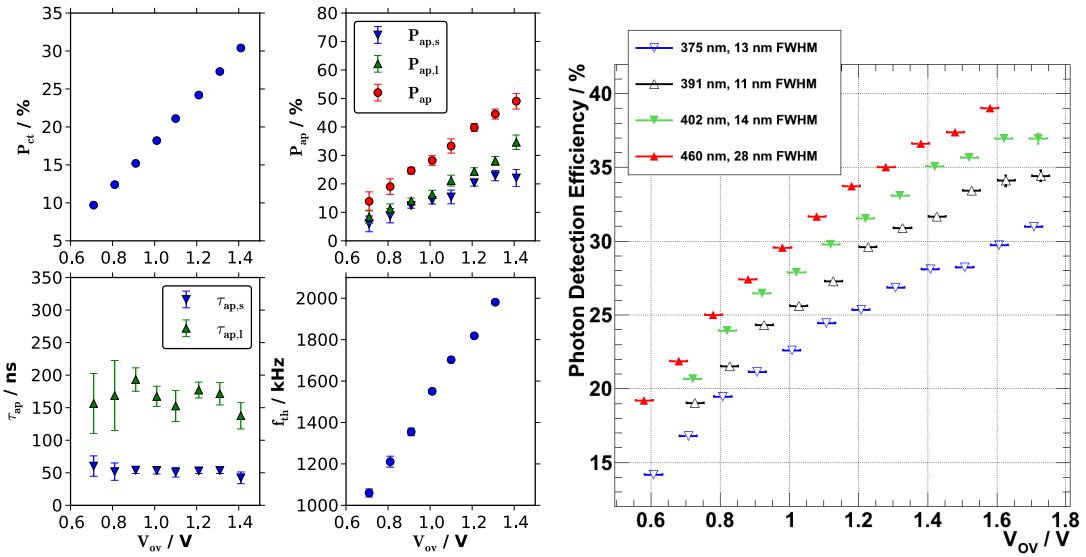

Figure 2.2.4: Important SiPM overvoltage dependencies. *Left*: The correlated noise crosstalk- (P_{ct}) and afterpulse-probability (short $P_{\text{ap,s}}$, long $P_{\text{ap,l}}$ and combined probability P_{ap}) and the corresponding afterpulsing time constants ($\tau_{\text{ap,l}}$ and $\tau_{\text{ap,s}}$) as functions of the over-voltage V_{ov} are shown. The thermal noise rate (f_{th}) as function of the overvoltage is given as well. For this measurement a Hamamatsu S10362-33-100C SiPM at ambient temperature T = (3.76 ± 0.03) °C was used. Taken from [16]. *Right*: Photon detection efficiency of a 1 mm x 1 mm, 100 µm cell pitch type SiPM for different peak emission wavelength [17].

optical crosstalk, produced by recombination of electron-hole-pairs, and afterpulsing, whereupon a delayed firing of cells is caused by a fired cell on account of impurities in the silicon substrate. For the afterpulsing-effect two time constants were found. In figure 2.2.4 the dependencies of the different noise phenomena from the overvoltage are shown. As it is prefereable to have a high PDE but low noise effects a compromise for the right overvoltage has to be found. Moreover, a stable overvoltage during the whole measurements is needed. Thus a overvoltage calibration as described in section 4.2 is necessary to operate the SiPMs with invariant characteristics.

One essential advantage of SiPMs is a competitive and even higher PDE, which was found to be in the range of 28% to 36% [17], in contrast to PMTs with approx 30%. With improving manufacturing processes, the PDE will increase and a dramatic suppression of thermal and correlated noise is expected [18]. Measurements at full moon or twilight may become possible leading to a higher duty cycle, since SiPMs are invulnerable to too much light. Moreover, SiPMs produce very fast signals at a high time resolution and are insensitive to magnetic fields. They have a low supply voltage under 100 V in comparison to PMTs. Because SiPMs are semiconductors a low-cost mass-production is possible, they have very small dimensions as seen in figure 2.2.3 and they are mechanically robust. A disadvantage of SiPMs is the strong temperature dependency, which can be controlled easily by temperature adapted bias-voltage by keeping the over-voltage constant. Moreover, the mentioned noise phenomena have to be considered. PMTs are also good for covering bigger areas out of one pixel, which is

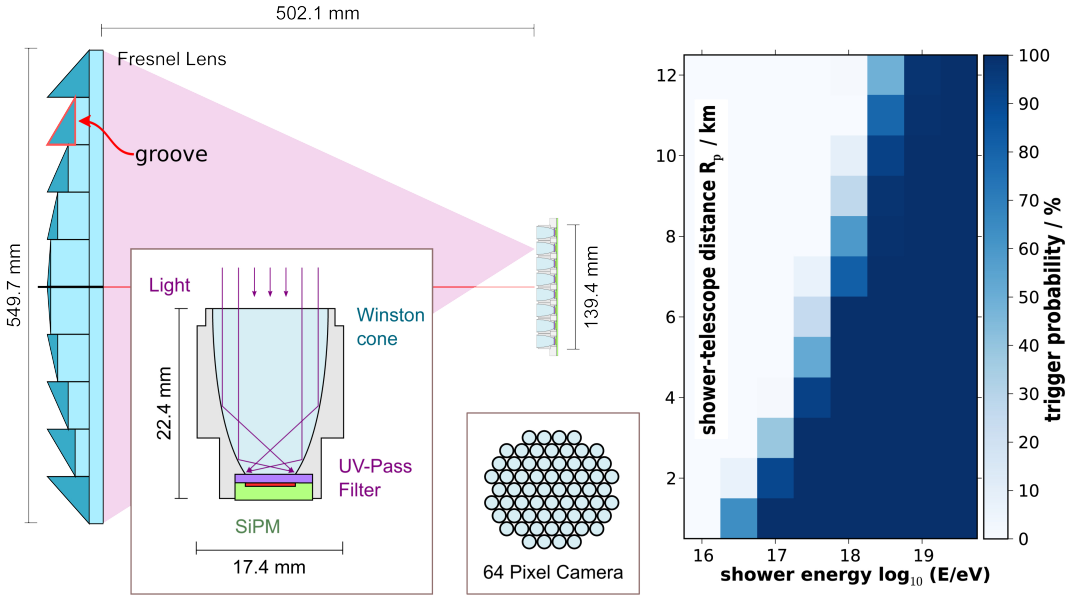

Figure 2.3.1: *Left:* Schematic design of FAMOUS with enlarged Fresnel lens. Adapted from [16]. *Right:* Extensive air shower trigger probability of FAMOUS simulated with Geant4 and CONEX. [16]

no issue for the purpose of air-shower fluorescence detection.

2.3 Baseline Design of FAMOUS

The air fluorescence telescope prototype FAMOUS has a simple refractive design. Incoming light is directly focussed onto the camera by a Fresnel lens. 64 SiPMs are hexagonally arranged in the focal plane, each behind an UV-pass filter and a light-concentrator as shown in illustration 2.3.1. Different studies and simulations for the Fresnel lens, the pixel design including characterisation of the used SiPMs and the overall performance as well as first test measurements have been done, showing the ability of FAMOUS to detect air showers (cf. right figure 2.3.1)[16].

2.3.1 Components of FAMOUS

Fresnel Lens The telescope concept with a Fresnel lens promises to have a high refraction power combined with small thickness and less absorption. Therefore the bulk lens material is divided in concentric annular sections, referred to as grooves, whose thickness is reduced to minimum. The used lens with 549.7 mm diameter and f = 502.1 mm focal length equal to the clear aperture transmits about 70 percent over the whole UV-regime and is made of acrylic with 10 grooves per millimeter (enlarged shown in figure 2.3.1). Raytracing simulations have revealed an aberration radius R_{90}[3] of 1.88 mm for a perfect lens for perpendicular incidence of parallel light.

[3] R_{90} is the radius including 90 % of encircled energy in the image plane

Camera The camera contains 64 non-imaging parabolic light concentrators, called Winston cones build of polished aluminum as schematically shown in figure 2.3.1. They gather the light with an entrance radius of 6.71 mm and concentrate it on a circular area with a radius of 3 mm. Winston cones are the best possible concentrators with a transmittance over 90% for a maximal incident angle of 26.6° [13]. Behind them 1 mm thin UV-pass filters[4] are placed in front of four 3 mm x 3 mm SiPMs[5] covering the whole output from the Winston cone.

Read Out Electronics All four channels of each pixel are combined to a sum signal via a Fan-In/Out. The SiPM charge is then converted to a digital signal by a CAEN V965 16 channel dual range *charge-to-digitial-converter* (QDC), which is read out via a Wiener VM-USB interface. The temperature adjusted bias voltage is set by a custom designed FTPC over RS-232. Both electronics are placed in a NIM-VME-combi-crate.

2.3.2 Famous[7]

The corresponding readout for all 64 channels and a programmable FPGA chip for triggering has been developed in Lisbon. Until the electronics are programmed and tested, the fully assembled and operational seven pixel version FAMOUS[7] gets extended to 64 pixel. A photo of the focal plane during the assembly of the seven pixel version and the assembled telescope is shown in figure 2.3.2. For now the 7 pixel version with in-house developed amplifiers is used for further studies and first measurement shifts in Aachen for test purposes. Therefore a DAQ combined with atmospheric sensors developed in this thesis is necessary.

[4] Schott UG-11
[5] Hamamatsu- S10985-100C SiPM

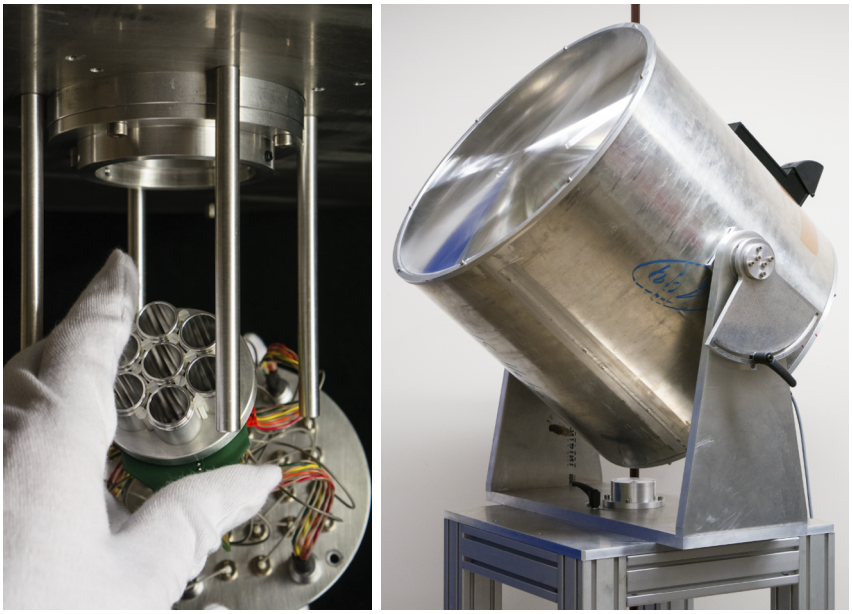

Figure 2.3.2: *Left:* Assembly of focal plane FAMOUS[7] prototype with SiPMs behind circular Winston cones. *Right:* Photo of assembled FAMOUS prototype with Fresnel lens and mount.

3 Data Acquisition for FAMOUS

Concerning the background information about UHECRs and FAMOUS[7], as presented in the chapter before, we are able to define the specifications of a Data Acquisition System (DAQ) exactly for this purpose. Based on these requirements the chosen components, their functions and connections are introduced. More over some basic tests and measurements for the environment sensors are documented and evaluated in respect of their use within the DAQ. At last the used software for Database and Data visualisation issues is shown and tested.

Data acquisition at the Pierre Auger Observatory

As a reference of a complex DAQ, the central data acquisition of the Pierre Auger Collaboration for the FD is briefly described. Since the gathering of data at the FD is only possible under certain environmental conditions, like a dark night with low wind speed and without rain, it is run in shifts, in which the crew has to ensure a proper operation. Therefore one central web-server at the campus in Malargüe provides a web interface for the remote access to the so-called *Slow Control System* (SCS) run on a PC in each of the four sites of the detector.

The SCS is connected to different sensors inside and outside the corresponding telescope building. The sensors outside gather information on the temperature, wind speed, humidity and light intensity to help the shifters to decide whether the current environmental condition is suitable for measurements. Inside each of the 6 telescope bays, sensors for the access doors, the luminance, the shutter, a failsafe curtain and the *Uninterruptible Power Supply* (UPS) are installed and monitored together with the outside sensors.

For safety reasons the SCS reacts to critical conditions and external errors autonomously. If necessary, it performs a proper shutdown or changes to a failsafe mode and it even starts up if the conditions are good again. Furthermore, only safe remote instructions of the web interface are accepted by the SCS. The obtained data is stored in MySQL databases in each site and then copied via replication mechanisms to a MySQL server at the campus in Malargüe together with the data from the SD. For more information see [19, 11].

3.1 Requirements

At first the desired DAQ should be connected to the existing electronics of FAMOUS[7], which are schematically shown in figure 3.1.1. Therefore a USB connection with an

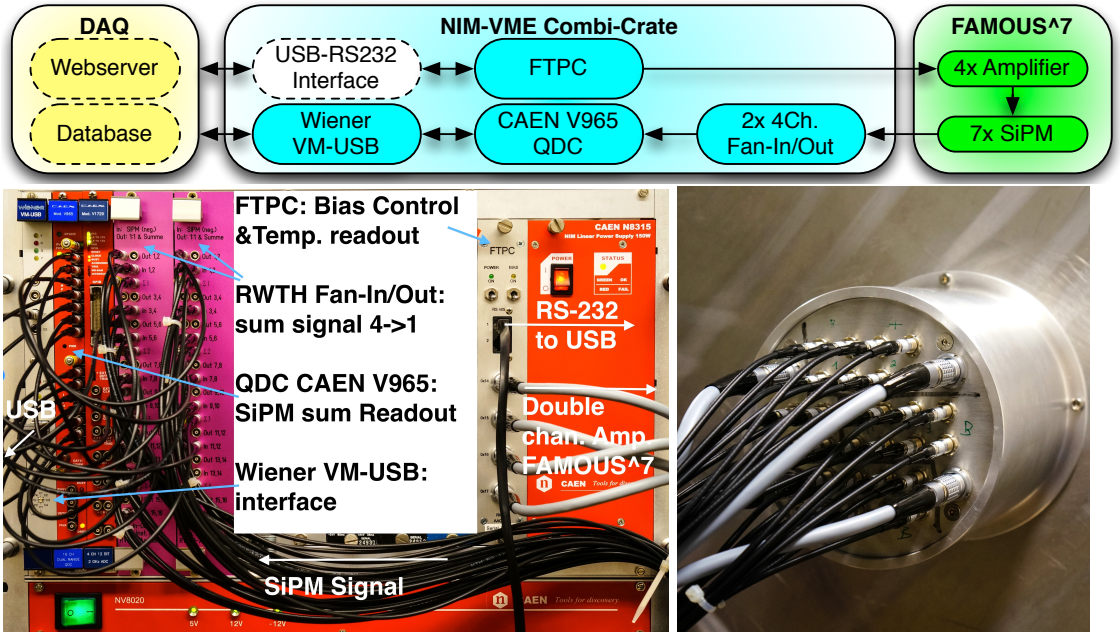

Figure 3.1.1: *Top*: Schematic diagram of the used read out electronics for FAMOUS[7]. *Bottom-Left*: Picture of FAMOUS[7] read out electronics in combi-crate as it is used for later test measurement (section 4.5) . *Bottom-Right*: Photo of wired 7 pixel version back-plate.

USB to RS232 interface to the FTPC, which was custom designed by RWTH-Aachen, is needed. With the FTPC module the bias voltage of each SiPM amplifier can be set and adjusted to the current temperature automatically. Furthermore, a temperature read out of the SiPMs is possible. All four channels of each SiPM are connected to an custom designed fan-in/-out also developed in-house. The sum-signal of each pixel is connected to the C.A.E.N V965 16 channel QDC. To readout the digitalised SiPM charge the QDC must also be connected to the DAQ via a Wiener VM-USB interface. First test, data readout and temperature controlled bias voltage routines are available as c++ code in the SiPM-library SiPM-Laboratory and should be executable on the DAQ.

Due to the robustness of SiPMs regarding too much light not that much safety mechanisms have to be included to the control as in the SCS of the Pierre Auger Collaboration. Additionally as a prototype FAMOUS is not fixed outside and no automated shutter has to be controlled.

To determine the environmental circumstances for better reconstructions of extensive air showers (cf. equation 2.2.2), sensors for temperature, air-pressure and humidity are desired. Moreover, a sensitive light-intensity sensor is useful to estimate the night-sky brightness. Hence the taken data should be associated with an accurate timestamp.

As the view and control part is critical and different settings, calibrations and scripts have to be combined for a full measurement, an user-interface is needed similar to the web-interface of the SCS at FD of the Auger observatory. This should also deliver fast access to the acquired data and current status of the experiment. An authorised

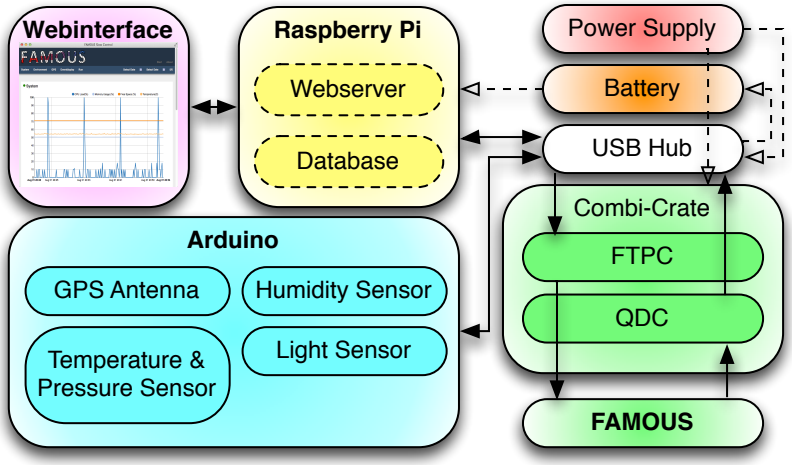

Figure 3.1.2: Schematics of the used elements and their communication (continuous lines) or electrical power flow (dashed lines) for the developed DAQ of FAMOUS.

remote connection via internet is of great advantage making the user independent from the experiment location. It also provides easy sharing and real time consultation with other researchers.

A fast and efficient database for the storage of taken data and the input of users is necessary. The database should be scaleable and indexable as well without consuming to much storage. Furthermore, replication or backup possibilities are useful for safety reasons. In order to display or download data fast and modifiable querying is requested.

The DAQ and the environment sensors should be small, as they are bound to the telescope. Additionally a portable solution for outdoor measurements is desired. Therefore an uninterruptible power supply build from an battery, which implies a small power consumption for the DAQ and the sensors, is a benefit. Besides a high mechanical stability for easy transport would be a good feature.

For the future use with the 64 pixels update, the chosen hard- and soft-ware should be easy scaleable. Optional easy setup and low-maintenance or rather simply replaceable components have been selected. Since the DAQ is only developed for the prototype FAMOUS a cheap solution, fulfilling the described requirements is preferred.

3.2 Components

Guided by the requirements the following components were selected and connected as shown in figure 3.1.2. As server, a small low-cost one-board computer, called *Raspberry Pi* (Pi), with linux as operating system was chosen. As central part of the DAQ the Pi (combined with a USB-Hub) is connected to all other components via USB and to the network via LAN and WLAN as well. So that the user controls everything on a computer over a webinterface as *Graphical User Interface* (GUI) via internet. On the Pi, an Apache webserver runs the webinterface querying the BSON [1] oriented database

[1] Binary JSON = Binary JavaScript Object Notation - A text-based open standard designed for human-readable data exchange.

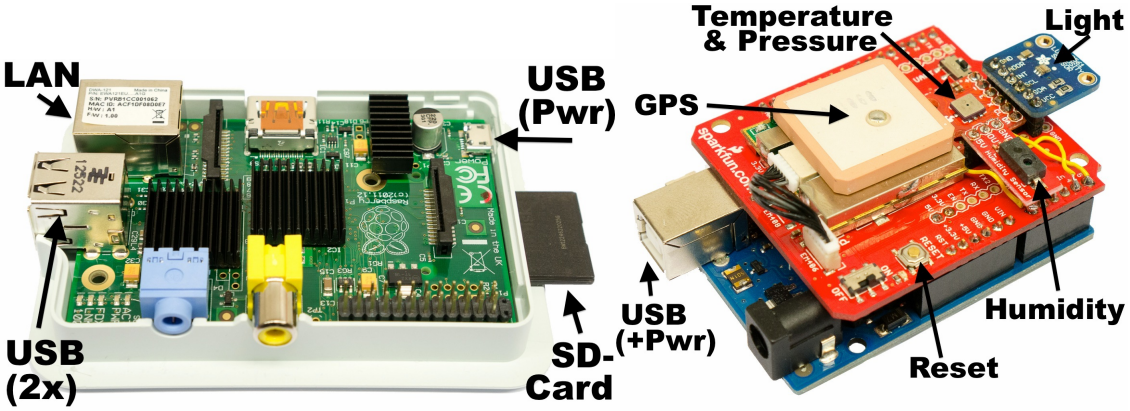

Figure 3.2.1: Photo of the Raspberry Pi in half-open box and the Arduino populated with Sensors outside the custom-made housing.

Mongo Db used for data handling. The SiPMs of FAMOUS are connected to the hub via existing and tested readout electronics (FTPC and QDC) located in a combi-crate. For up-to-date environment data the single-board micro-controller Arduino is equipped with a infrared and broadband luminosity sensor, a humidity sensor, a combined temperature and pressure sensor and a GPS antenna for exact timing. The consolidated sensor device based on an Arduino board is also connected to the Pi via USB.

3.2.1 Raspberry Pi Mini Computer

The Raspberry Pi is a credit-card-sized computer developed by the Raspberry Pi foundation. It has a 700MHz CPU, which can securely and automatically be overclocked to 1GHz, 512 MB RAM, two USB Ports and one ethernet port as shown in photo 3.2.1. So it can be connected to the FAMOUS readout electronics easily via USB and controlled over the ethernet port. Additionally a wireless LAN USB stick is connected to a USB port of the USB hub. The operating System , Debian GNU/Linux 7.1, is installed on a 32Gb SD-Card. For additional storage a larger SD-Card can be used or USB hard disks can be connected. The Pi is programmed over network via ssh. First tests have shown, that the Raspberry Pi is fast enough to handle the existing SiPM readout scripts and store the data in a database, as the incoming data is buffered by the QDC until readout. The web-platform runs responsive as well. As power supply the 5V micro USB input is connected to a 2000 mAh battery, which is constantly charged by the powered USB hub. When the power for the hub fails, the battery takes over and delivers power for long, so that safety mechanisms can be installed and a controlled shutdown can be executed directly. An additional restart switch is installed for easy resets of the Raspberry Pi. With dimensions of 85 mm x 56 mm the Pi is portable and can be mounted directly to the telescope. The expandability to the 64 pixel version of FAMOUS is only limited by the software.

3.2.2 Arduino Microcontroller and Environment Sensors

An Arduino Uno (revision 3) board is used to collect the data of environment sensors. This open-source electronics prototyping platform has a 16 Mhz clock processor, 32 kB of storage, 6 analog inputs, 14 digital pins and can be easily connected and programmed via USB using a language and libraries based on the Wiring[2] language similar to C++. In figure 3.2.1 the Arduino with its sensors soldered to a GPS shield is shown. To protect the electronics a custom designed housing was developed with a transparent top for the light sensor. Additionally a controllable fan is designated, so that the board reacts faster to environmental changes and is protected from condensation. In the following, the used sensors are described and a noise measurement of each sensorvalue with 30 s measure time at its fastes refreshrate is presented. The time tracess for all sensor values can be found in the appendix. In the continuous running duty the sensor values are taken every 10 s and stored in the database.

GPS-Shield and GPS-receiver A GPS-shield is plugged on to the Arduino to connect the GlobalSat 20 channel EM-406A SiRF III GPS-receiver [20] including antenna. The GPS enables the Arduino to obtain a very precise timestamp and to sync the system time of the Raspberry Pi without internet connection. As portable prototype the GPS position is also a useful feature. Noise measurements of the longitude, latitude, height and satellite shown in figure 5. The number of satellites shows, that always enough satellites are seen, although the measurement was done inside. To calculate the accurancy distance d of the position in latitude and longitude (α) can be estimated by geometry and the mean Earth radius R_{Earth} with $d = R_{\text{Earth}} \cdot \alpha \cdot \frac{\pi}{180^\circ}$. So that the measured standard deviation in latitude and longitude correspond to 9.8 m and 9.1,m accuracy. The GPS-shield also provides a prototyping area which is used to fix the sensors to the Arduino.

Light-sensor As luminosity sensor a TAOS TSL2561[21] is used, containing a infrared and a full spectrum diode. Since the human eye can not perceive infrared light that is detected by most photo diodes, the extra infrared diode is needed to subtract the infrared fraction. This allows the software to compute real lux values for human-visible light. The sensor has two integrating *analog-to-digital converters* (ADCs) with different gain (1x and 16x) and integration time window (13ms, 101ms and 402ms) settings, so that a light range from $1\,lx$ to $40,000\,lx$ is achieved. The two ACD values in arbitrary units can be read out and are ploted in the noise measurement plots too. The formula used to calculate the lux value depends on ADC count of the infrared channel n_{infra} divided by the ADC count of the broadband channel n_{broad}. Basicly the broadband channel and infrared channel are scaled with empiric values and then the infrared value is subtracted from the broadband value. For example the lux value l in one range can be calculated with the following formula.

$$0.80 < \frac{n_{\text{infra}}}{n_{\text{broad}}} < 1.30 \qquad\qquad l = 0.00338 \cdot n_{\text{broad}} - 0.00260 \cdot n_{\text{infra}}$$

[2] http://wiring.org.co

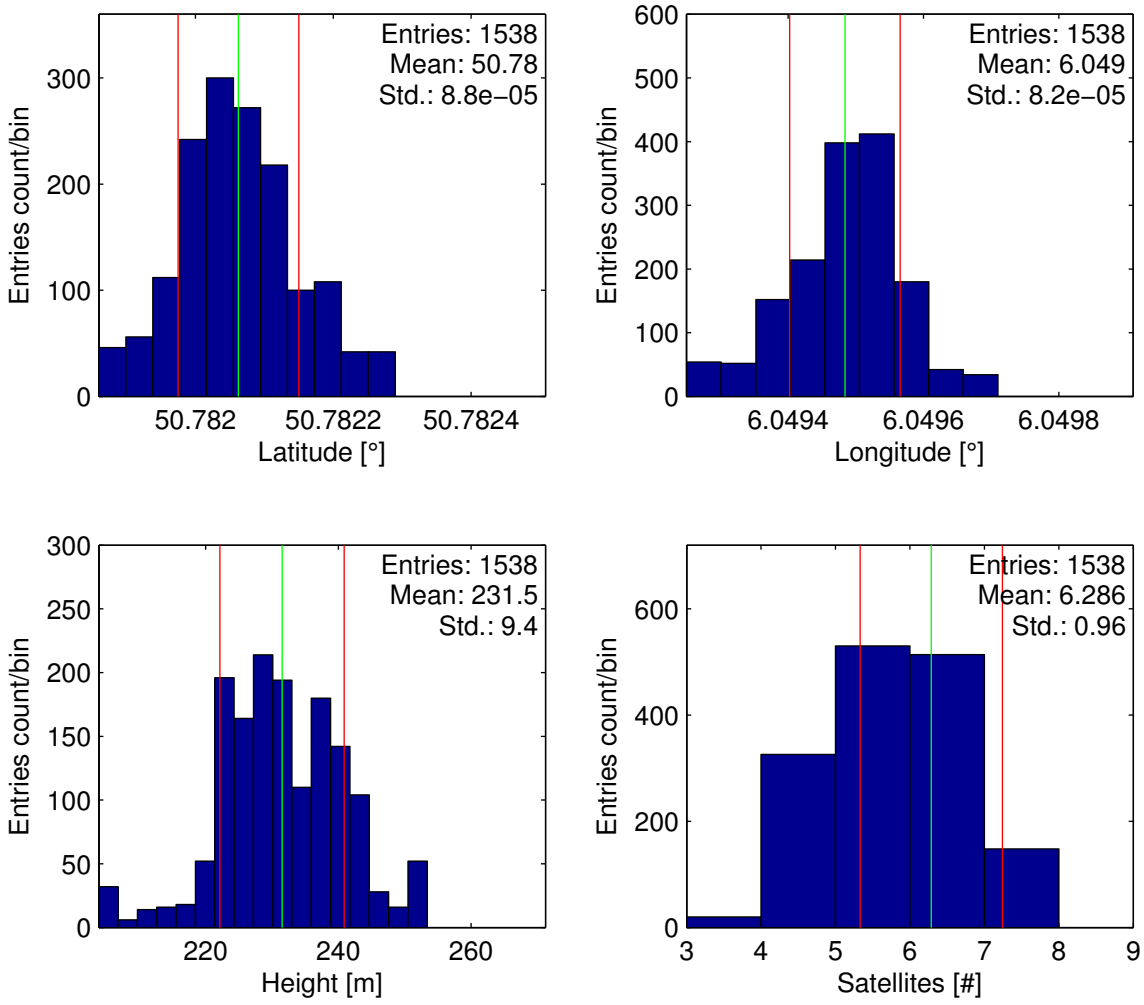

Figure 3.2.2: Noise measurements of the GPS-reciever connected to the Arduino.

Only in one of four ranges an additional correction factor has to be applied.

$$0 < \frac{n_{\text{infra}}}{n_{\text{broad}}} < 0.52 \qquad l = 0.0315 \cdot n_{\text{broad}} - 0.0593 \cdot n_{\text{broad}} \cdot (\frac{n_{\text{infra}}}{n_{\text{broad}}})^{1.4}$$

The light sensor is connected to the Arduino via the digital I^2C-bus. The noise measurements were done with 13ms integration time and without gain (1x). Therefore the step-width is one lux, which can be seen in the measurement plot. The standard deviation is very low with $0.73\,lx$ for human eye illuminance, so that the sensor is precise enough to distinguish between a dark and a bright night.

Pressure and Temperature Sensor A combined pressure and temperature sensor, the Bosch BMP-085 [22], is connected to the Arduino via the digital I^2C-bus as well. It can measure the barometric pressure in a range from 300 hPa to 1100 hPa and is fully calibrated, so that no translation for the digital values is needed. Pressure and temperature can be read with a precision of 16bit[3]. A digitalisation effect is seen in the

[3] 16 bit = 2^16 =65536 individiual values in the measurement range

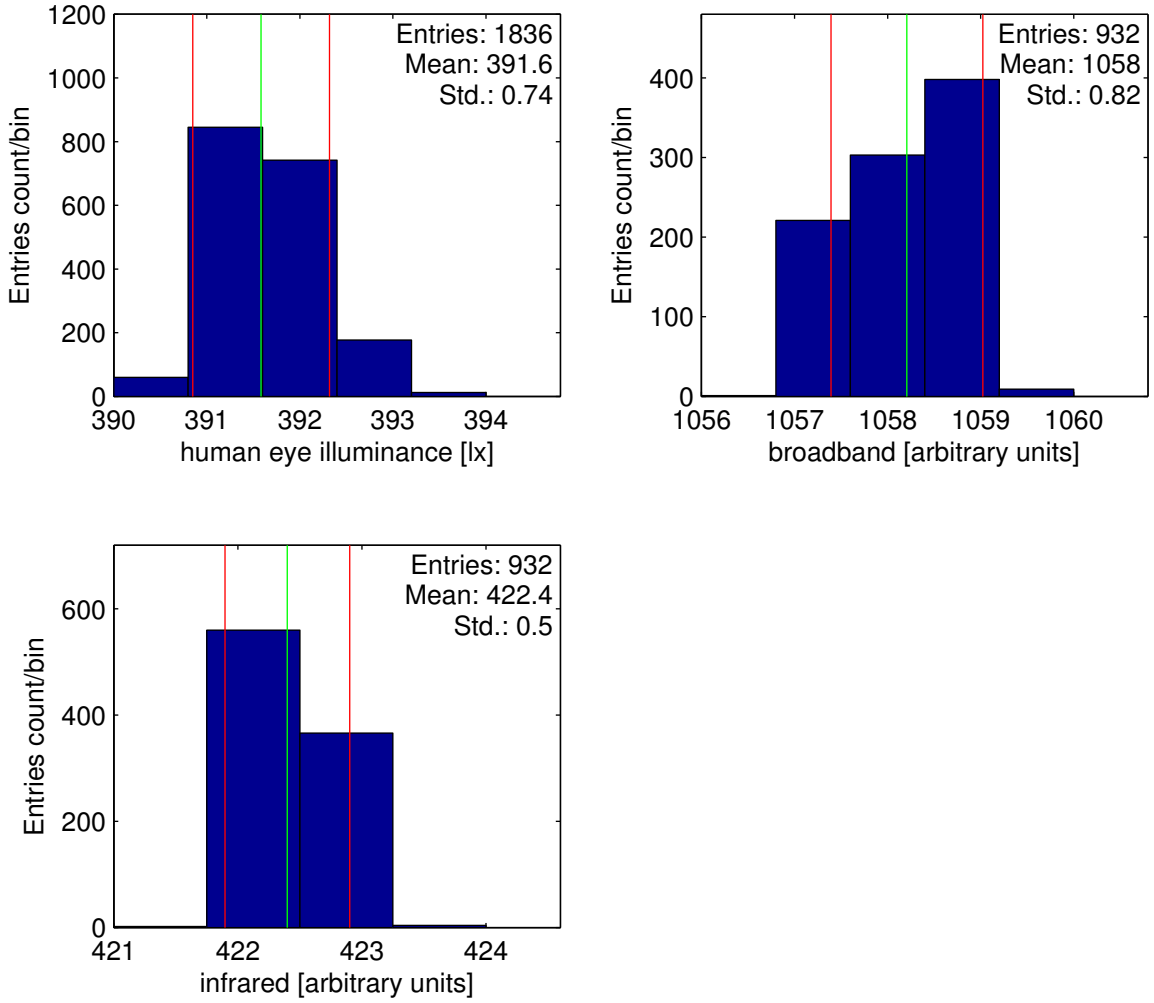

Figure 3.2.3: Noise measurements of the light-sensor connected to the Arduino.

temperature noise measurement plot. With a standard deviation of about 0.01°C the temperature is measured with enough precision. The measured standard deviation for pressure is 3.5 Pa which is as smaller as the accuracy given by the manufacturer with 3 Pa (RMS noise). So the BMP085 is precise enough to determine the current weather situation.

Humidity Sensor To measure the humidity, a Honeywell HIH-4030 [23] sensor is connected to an analog input of the Arduino or rather the GPS-shield. The sensor operates in a range of 0 to 100% relative humidity and has a fast response time of 5 s. Because the voltage-humidity-slope depends a slightley on the temperature, the sensor value is adjusted by the temperature read from the BMP085 sensor and the calibration values given from the manufacturer. Therefore, the analog voltage V_{out} is read and converted to the adjusted relative humidity u_{adj} via following formula.

$$u_{\text{adj}} = \frac{\frac{V_{\text{out}}}{V_{\text{supply}}} - 0.16}{6.539 - 0.013392 \cdot T[^{\circ}C]} \cdot 1000$$

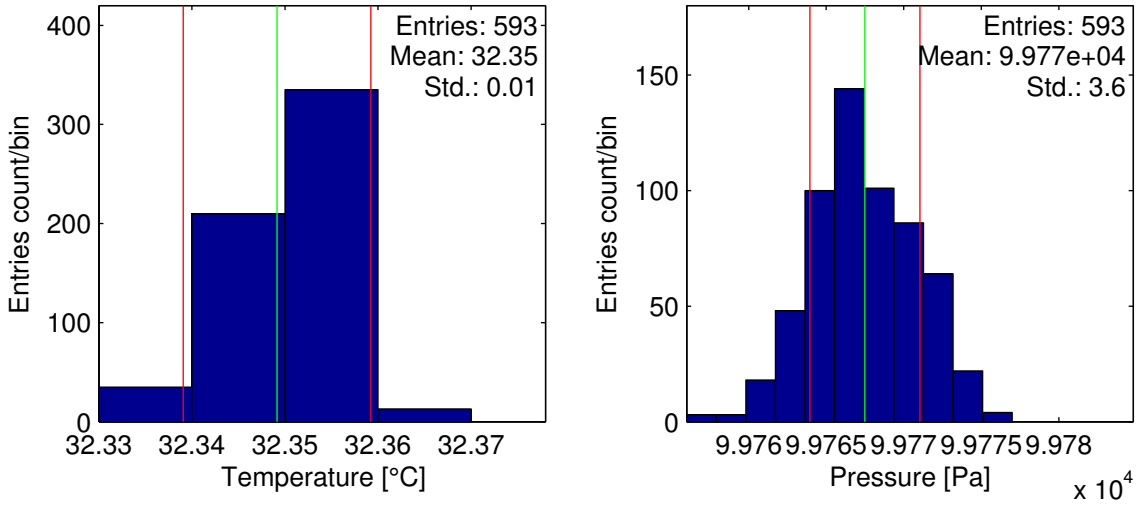

Figure 3.2.4: Noise measurements of the pressure and temperature sensor connected to the Arduino.

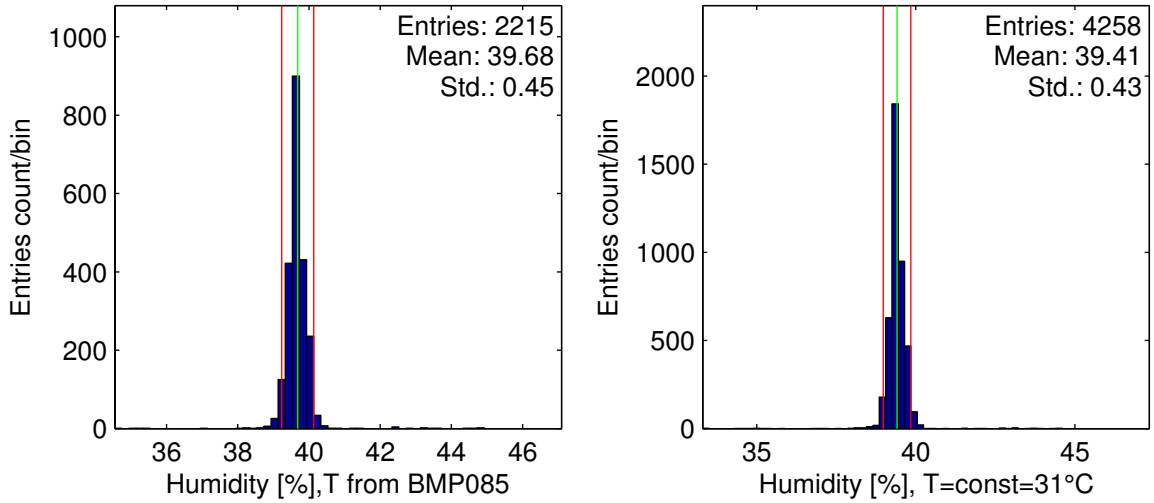

Figure 3.2.5: Noise measurements of the humidtiy sensor connected to the Arduino.

The measured standard deviation of 0.45% relative humidity with temperature adjusted values is very low. As the temperature variance of BMP-085 value is verry low and because it is a weak temperature dependency, the standard deviation with a fixed temperature value is only 0.04% (relative humidity) lower. These values are much smaller than the accuracy of the best fit straight line given by the manufacturer with 3.5% relative humidity.

Summary The following table sums up all measured sensor values and the reference values from the manufacturers as denoted in their specifications. Altogether, the used sensors fulfill the requirements and work together with the DAQ. Thus the environement sensors are fully operational and the taken data is stored in a database continuosly.

Sensor	Value	σ	Reference	Comment
GPS-reciever EM-406A	latitude	9.8 m	10 m	2D RMS
	longitude	9.1 m		
	height	9.4 m		
	number of satellites	1		
Light sensor TSL2561	human-eye illuminance	0.73 lux	0.1 lux	at high gain(16x)
	brodband	0.82 a.u.		
	infrared	0.50 a.u.		
Temperature & Pressure sensor BMP-085	temperature	0.01 °C	(2.5 °C)	(whole temperature and pressure range)
	pressure	3.5 Pa	3 pa	RMS Noise
Humidity sensor HIH-4030	humidity (T adjusted)	0.45 %	0.5 %	repeatabillity
	humidity (T constant)	0.41 %		

Table 3.2.1: Measured sensor values and manufacturers specifications.

3.3 Database and Web-interface

Since the data has to be stored properly a document orientated Database, MongoDB from 10gen incorporation, was chosen to be installed on the Raspberry Pi. Its advantages in contrast to the requirements are discussed in the following. After that the developed webinterface is shown in detail.

3.3.1 MongoDB

The open-source document database MongoDB (from "humongous") is easy to install on the unix system running on the Raspberry Pi and is the leading NoSQL-database [24]. Since the data is stored in a BSON-formated documents it is human readable and easy to combine different information and group them in subdocuments and arrays. The records are stored in collections in different databases. The Arduino and the readout scripts were programmed to send the data in BSON-format, so that the output can be directly stored in the database. An example document created by the Arduino is presented in figure 3.3.1.

MongoDB provides fast access to the data and has the ability to index on any attribute, like the GPS-time stamps. Combined with a powerful and simple querying language it is easy to find data, based on nearly any criterion. For each data entry an unique Id-object is created containing a timestamp, machine identifier, system process id and a continuous counter, so that each document can be safely accessed. In the database for FAMOUS collections for the Raspberry Pi system statistics, the environment data from Arduino, triggered events, calibrations and shift data are installed. A database request to find a document in the system collection by a specific date and time with over one million entries in it only lasts 2.5ms on average. This test was performed with 10000 requests, querying for the indexed date and time. Some test data (around 1.5 million entries) only took 280mb of storage, showing the efficiency of MongoDBs storage engine. Moreover, MongoDB provides replication mechanisms, so that the

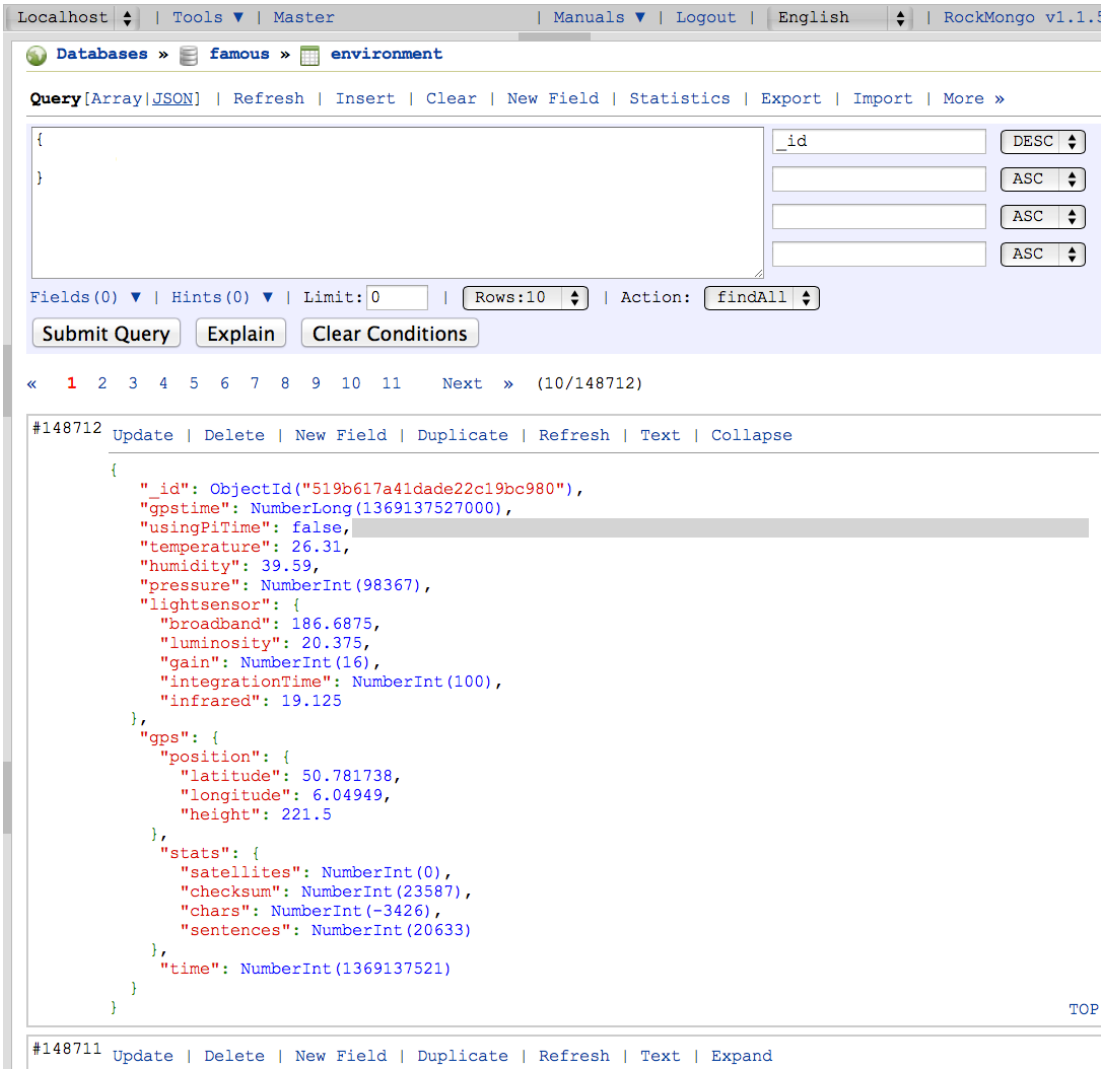

Figure 3.3.1: Screenshot of Rockmongo, an administration tool for MongoDB, showing some environment data.

whole database can be mirrored to another server. To easily administrate the database the server application "Rockmongo" is installed, which can also be seen in figure 3.3.1.

3.3.2 Webinterface

The webinterface is programmed with PHP and connects to MongoDB via the PHP-MongoClient to load and store the selected data. To reduce the CPU-usage of the Raspberry Pi, many parts of the webinterface use client-side executed Javascript as for example the presentation of the recorded data in plots. The obtained data is visualised by scripts from Data-Driven-Documents (D3)[4]. In the following the different webpages are described and presented by the use of screenshots.

[4] http://d3js.org

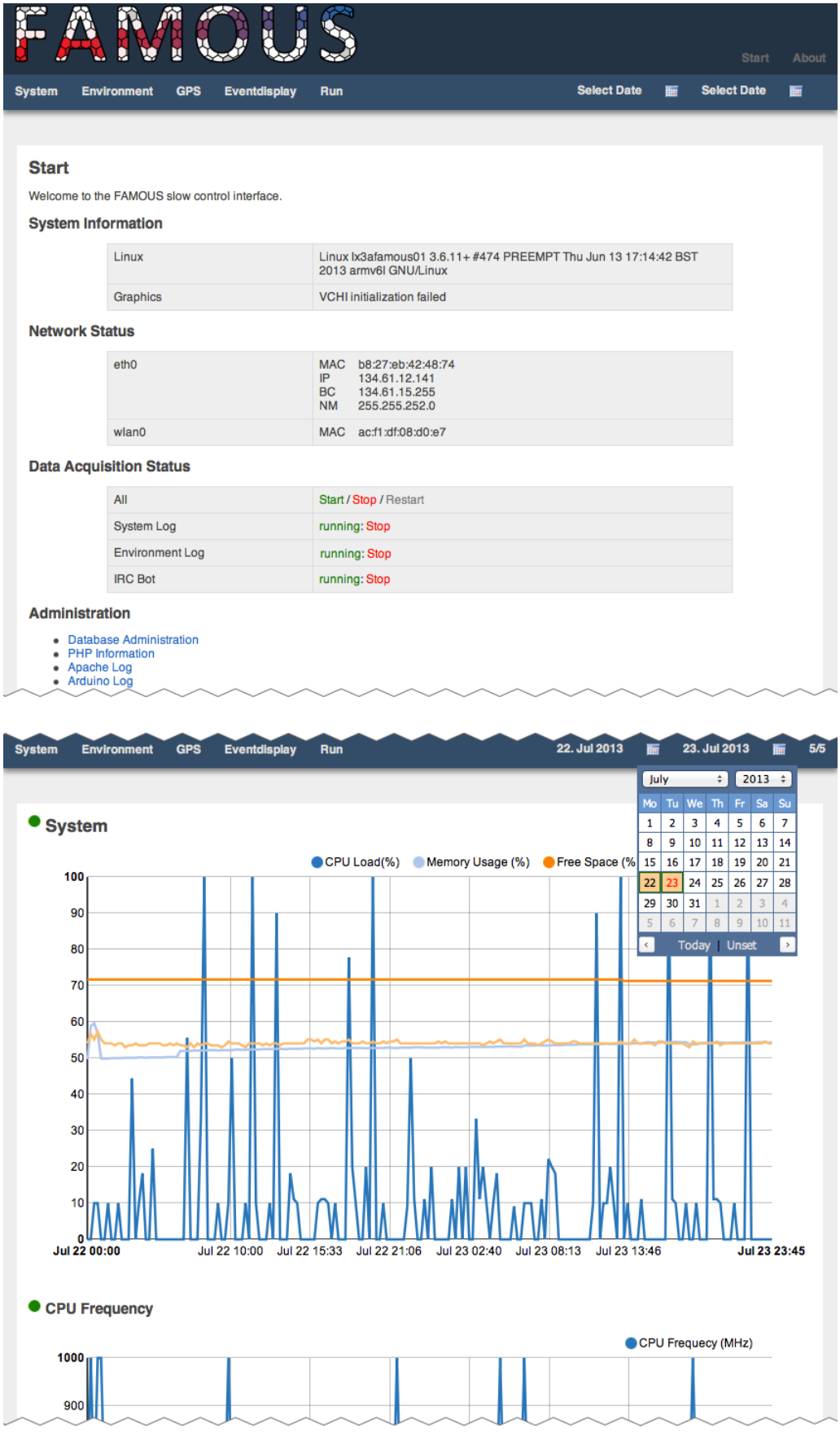

Figure 3.3.2: Screenshots of the "Start" and "System" page of the FAMOUS DAQ interface.

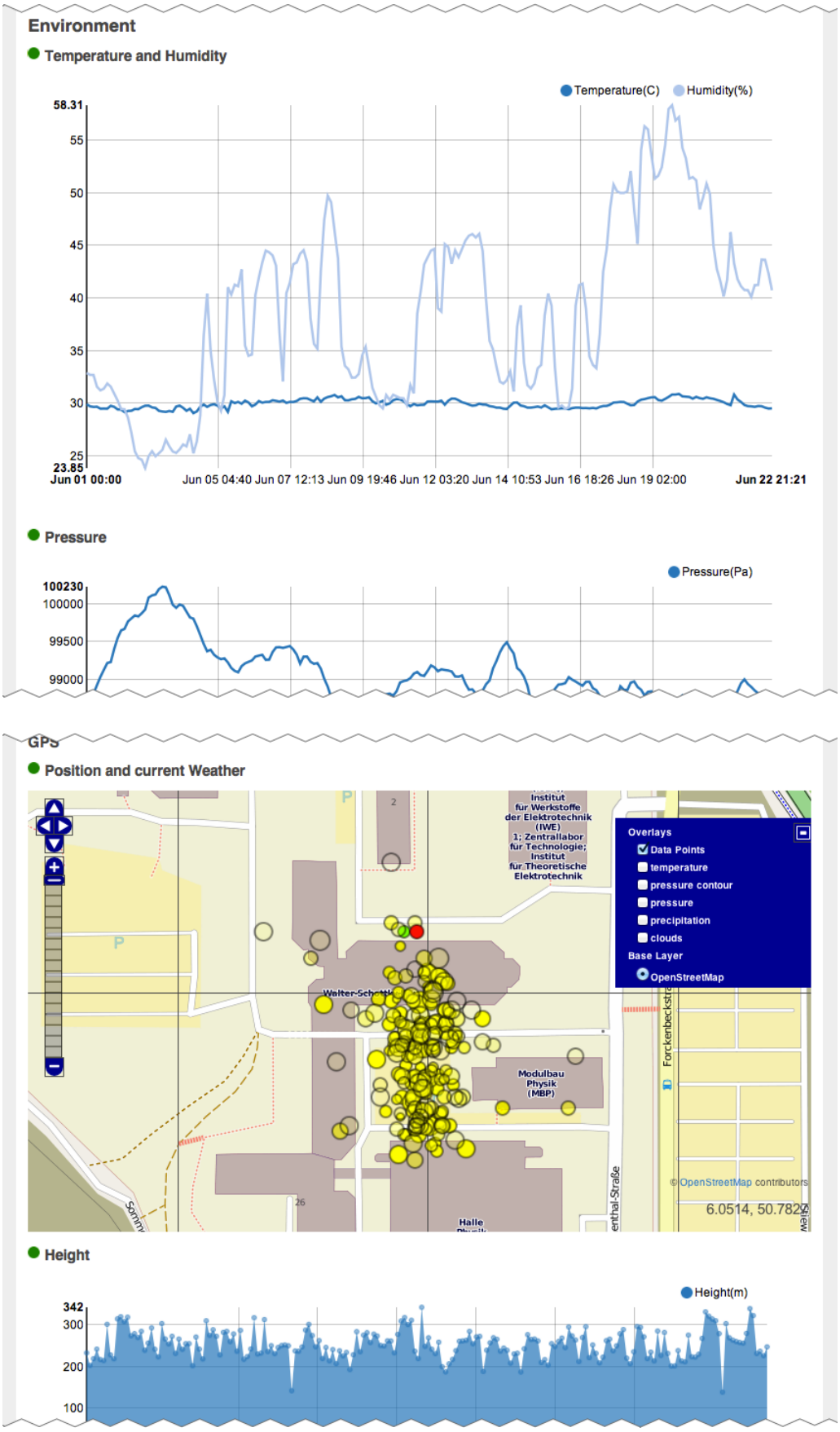

Figure 3.3.3: Screenshots of the "Environment" and "GPS" page of the FAMOUS DAQ interface.

The "Start" page offers basic status information about the Raspberry Pi and its network status. Also the scripts for system log, environment log and a IRC-bot can be started and stopped from here. Moreover, different links to the Apache server log, PHP information, Arduino-connection log and Rockmongo database administration tool are given. Detailed information on the Raspberry Pi from the system collection like board-temperature, CPU-load, CPU-frequency, memory usage and free space are shown on the "System" page. The displayed data range can be selected by two small calendars in the top bar and is written back in the URL for easy access and linking. Every diagram has a red, yellow or green circle next to it indicating the status of the current data request. Always 200 data points in the data range or the last 200 data points if no range is specified are displayed. In multiple plots each data series can be selected at the diagram top. The System page also shows database statistics for MongoDB including data size and number of objects for example.

Data from the Arduino board is divided into an "Environment" and a "GPS" page. These pages show the temperature, pressure and light values on the "Environment" page and GPS position, height, number of satellites, and the time-fix on the "GPS" page. For the GPS position a Open Layers Map[5] is used showing the last 64 positions time color coded and with point-radius coded number of satellite fixes. Additionally the current weather situation can be displayer via different layers. Thus it is possible to see the current temperature, pressure, rain probability and cloud distribution at a wider scale of the map.

Since the telescope is operated at night, it is important to know details about the moon-phase, as the moon lightens the night-sky. Hence a webpage, presented in figure 3.3.4, about the moon, showing the moon fraction, its rise and set time and even the sunrise and set times. To calculate these values the date, time and last known position of the GPS sensor are used automatically or can be entered manually to the designated fields. Then the moon fraction for example is a simple geometrical calculation. For an overview over a whole year, the nautical and astronomical twilight, the moon rise and set times and the moon-fraction can be calculated by a script of the United States Naval Observatory (USNO).

The two pages "Eventdisplay" and "Run" are described in the next chapter (4.1, 4.4) in detail.

For further communication with the Arduino and basic stats, like the IP address, an IRC[6] bot is established. An IRC bot is an independent program that connects to Internet Relay Chat as a client, and so appears to other IRC users as another user. Over the serial connection to the Arduino the sensor data, current time, time status can be obtained and custom commands can be send to the Arduino. Moreover, the auto gain, gain and integration time for the light-sensor can be controlled. With the command "Arduino help" a full command list from the Arduino is returned. For debugging the log-level for the Arduino connection log can also be set by the IRC-bot.

[5] http://openlayers.org

[6] IRC = Internet Relay Chat, a protocol for live interactive Internet text messaging (chat) or synchronous conferencing.

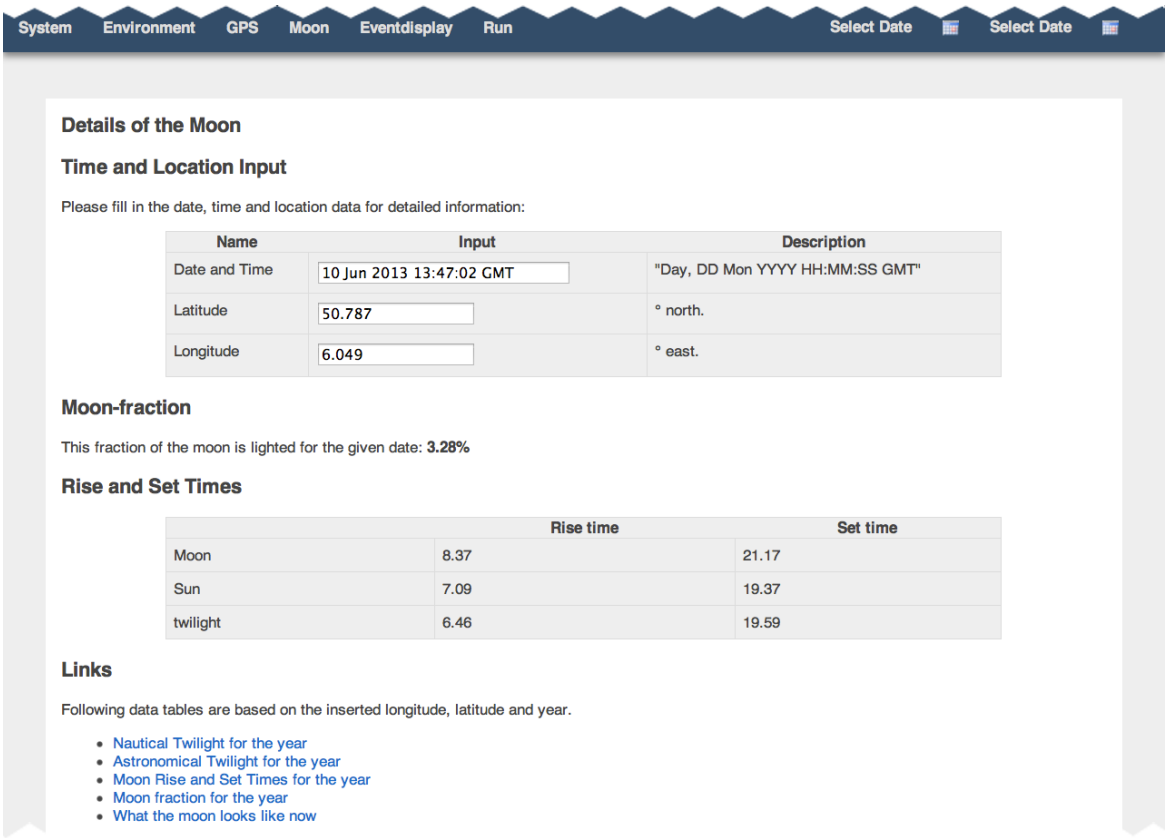

Fraction of the Moon Illuminated, 2013
at Midnight
Zone: 2h East of Greenwich

Astron. Applications Dept.
U. S. Naval Observatory
Washington, DC 20392-5420

Day	Jan.	Feb.	Mar.	Apr.	May	June	July	Aug.	Sep.	Oct.	Nov.	Dec.
01	0.89	0.78	0.89	0.75	0.67	0.49	0.43	0.30	0.19	0.17	0.08	0.06
02	0.82	0.68	0.81	0.65	0.56	0.38	0.33	0.21	0.12	0.10	0.03	0.02
03	0.73	0.58	0.72	0.53	0.45	0.28	0.24	0.14	0.07	0.05	0.01	0.00
04	0.63	0.46	0.61	0.42	0.34	0.20	0.16	0.08	0.03	0.01	0.00	0.01
05	0.53	0.35	0.50	0.31	0.25	0.13	0.10	0.04	0.00	0.00	0.03	0.05
06	0.42	0.25	0.39	0.21	0.16	0.07	0.05	0.01	0.00	0.01	0.08	0.12
07	0.31	0.15	0.28	0.13	0.09	0.03	0.02	0.00	0.02	0.04	0.15	0.21
08	0.21	0.08	0.18	0.07	0.04	0.01	0.00	0.01	0.06	0.10	0.24	0.31
09	0.12	0.03	0.10	0.02	0.01	0.00	0.01	0.04	0.13	0.18	0.35	0.42
10	0.05	0.00	0.05	0.00	0.00	0.02	0.03	0.09	0.21	0.27	0.46	0.53
11	0.01	0.01	0.01	0.00	0.01	0.05	0.06	0.16	0.30	0.38	0.58	0.64
12	0.00	0.03	0.00	0.02	0.03	0.09	0.12	0.24	0.41	0.50	0.68	0.74
13	0.02	0.08	0.01	0.06	0.08	0.16	0.19	0.34	0.52	0.61	0.78	0.82
14	0.06	0.15	0.05	0.12	0.13	0.23	0.28	0.44	0.64	0.72	0.86	0.89
15	0.13	0.23	0.10	0.18	0.20	0.32	0.37	0.55	0.74	0.81	0.93	0.94
16	0.21	0.32	0.17	0.26	0.29	0.42	0.48	0.66	0.84	0.89	0.97	0.98
17	0.30	0.41	0.25	0.35	0.38	0.52	0.59	0.77	0.91	0.95	0.99	1.00
18	0.40	0.51	0.33	0.44	0.47	0.63	0.69	0.86	0.97	0.99	1.00	1.00
19	0.49	0.60	0.43	0.54	0.57	0.73	0.79	0.93	0.99	1.00	0.98	0.98
20	0.59	0.69	0.52	0.64	0.67	0.82	0.88	0.98	1.00	0.99	0.95	0.94
21	0.68	0.77	0.61	0.73	0.77	0.90	0.95	1.00	0.97	0.96	0.90	0.89
22	0.76	0.85	0.70	0.82	0.86	0.96	0.99	0.99	0.93	0.91	0.84	0.83
23	0.84	0.91	0.79	0.89	0.93	0.99	1.00	0.95	0.87	0.85	0.76	0.75
24	0.90	0.96	0.86	0.95	0.98	1.00	0.98	0.90	0.79	0.78	0.68	0.66
25	0.95	0.99	0.93	0.99	1.00	0.97	0.93	0.82	0.71	0.69	0.59	0.57
26	0.98	1.00	0.97	1.00	0.99	0.91	0.86	0.74	0.62	0.60	0.49	0.47
27	1.00	0.99	1.00	0.98	0.95	0.83	0.78	0.64	0.52	0.51	0.39	0.36
28	0.99	0.95	1.00	0.94	0.89	0.74	0.68	0.55	0.43	0.41	0.30	0.26
29	0.97		0.97	0.87	0.80	0.64	0.58	0.45	0.34	0.32	0.21	0.17
30	0.92		0.92	0.78	0.70	0.53	0.48	0.36	0.25	0.23	0.13	0.09
31	0.86		0.84		0.60		0.39	0.27		0.15		0.04

Figure 3.3.4: Screenshots of the Moon page of FAMOUS webinterface and a year overview table of the moon-fraction calculated by a script from the United Stated Naval Observatory based on the same date and position values.

4 Recording Sequence

To record data with the DAQ consisting of the software and hardware described in the chapter before, measurements are started in a defined *run* Sequence. This ensures data integrity and standardised data output for better analysis and easy database storage. Moreover, this avoids errors in controlling the telescope due to failsafe mechanisms and a clearly defined sequence of steps to make FAMOUS ready for recording events including calibrations for the SiPMs. The run sequence also contains a stop procedure to end the measurement properly and shutdown every component correctly. It is shown how event recording and displaying is possible over the DAQ webinterface via network, using the capabilities of the Raspberry Pi.

4.1 Run Sequence

To start a new measurement, referred to as run or shift, the "Run" page of the FAMOUS webinterface can be used if no run is on duty. The following five steps have to be completed to start a shift, as documented from figure 4.1.1 to 4.1.4.

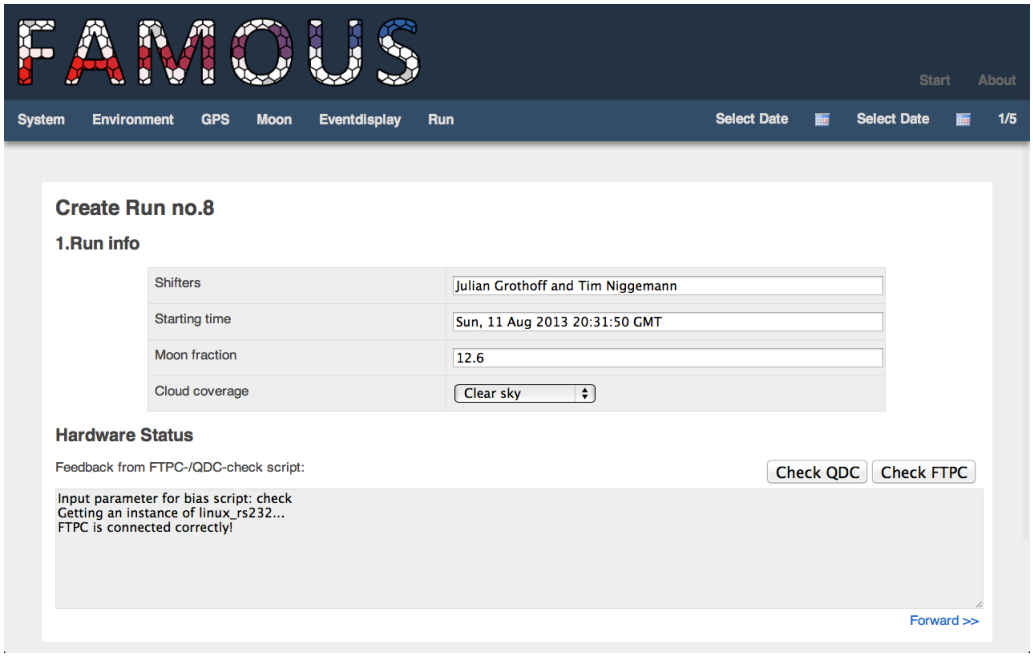

Figure 4.1.1: Screenshot of the first step of the start sequence, containing the basic information of the new run and hardware checkups.

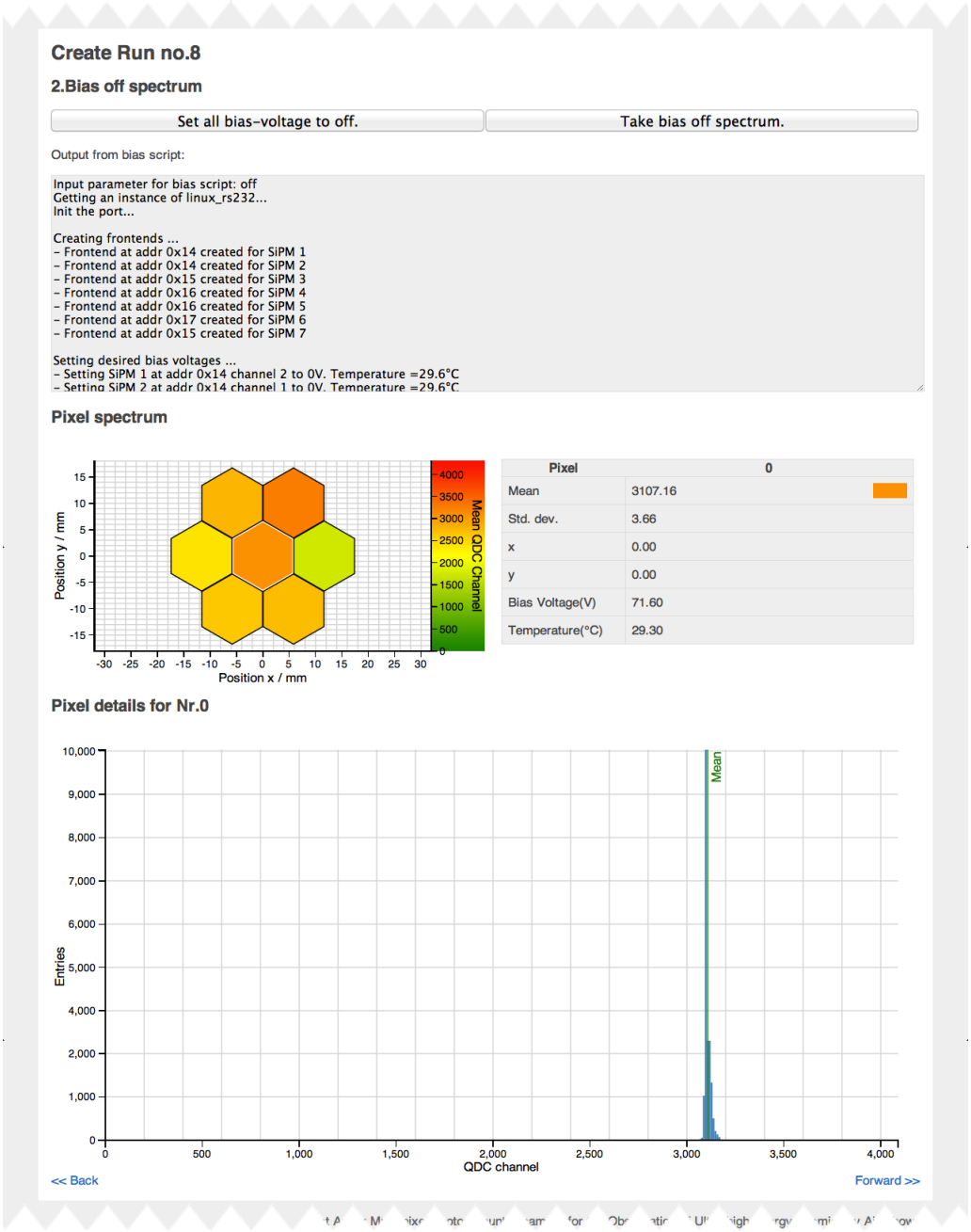

Figure 4.1.2: Screenshot of the second step of the start sequence, containing the measurement of the QDC spectrum while bias-voltage is turned off.

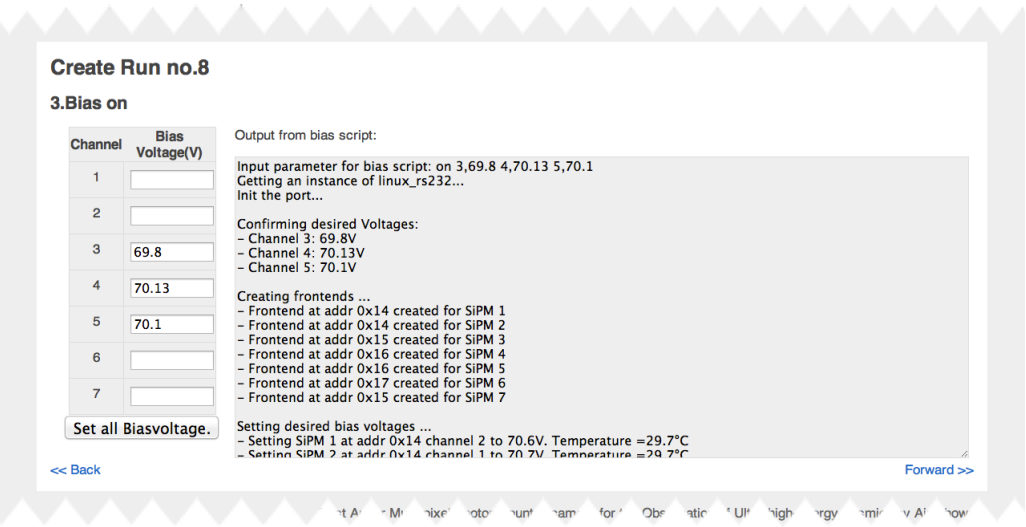

Figure 4.1.3: Screenshot of the third step of the start sequence, containing the setup of custom bias-voltages.

Figure 4.1.4: Screenshot of the last step of the start sequence, containing the over-voltage selection and the actual start of the measurment.

- At first the basic information such as the names of the shifters, the current time and the weather conditions in the form of standardised cloud coverage selection is protocolled. The moon fraction can be obtained from the "Moon" page of the DAQ interface. Moreover, the hardware connection status of FAMOUS read out electronics is displayed after pressing the corresponding buttons. Therefore basicly the connection to the FTPC and to the QDC is tested.

- During the second step the bias-voltage is set to zero and a QDC spectrum is taken. A field for feedback from the started bias and QDC scripts is integrated beneath the script start buttons showing the commandline output. This spectrum is used as reference or noise background and can be subtracted from the measurements later. The last taken spectrum is stored in the MongoDB and can be inspected in the same way as described in the eventdisplay section (4.4) right in this place.

- The third step delivers the opportunity to set individual bias-voltages at 25°C for every pixel. If no voltage is given, the default values from bias script are used. After setting the voltages by the corresponding button, the output from

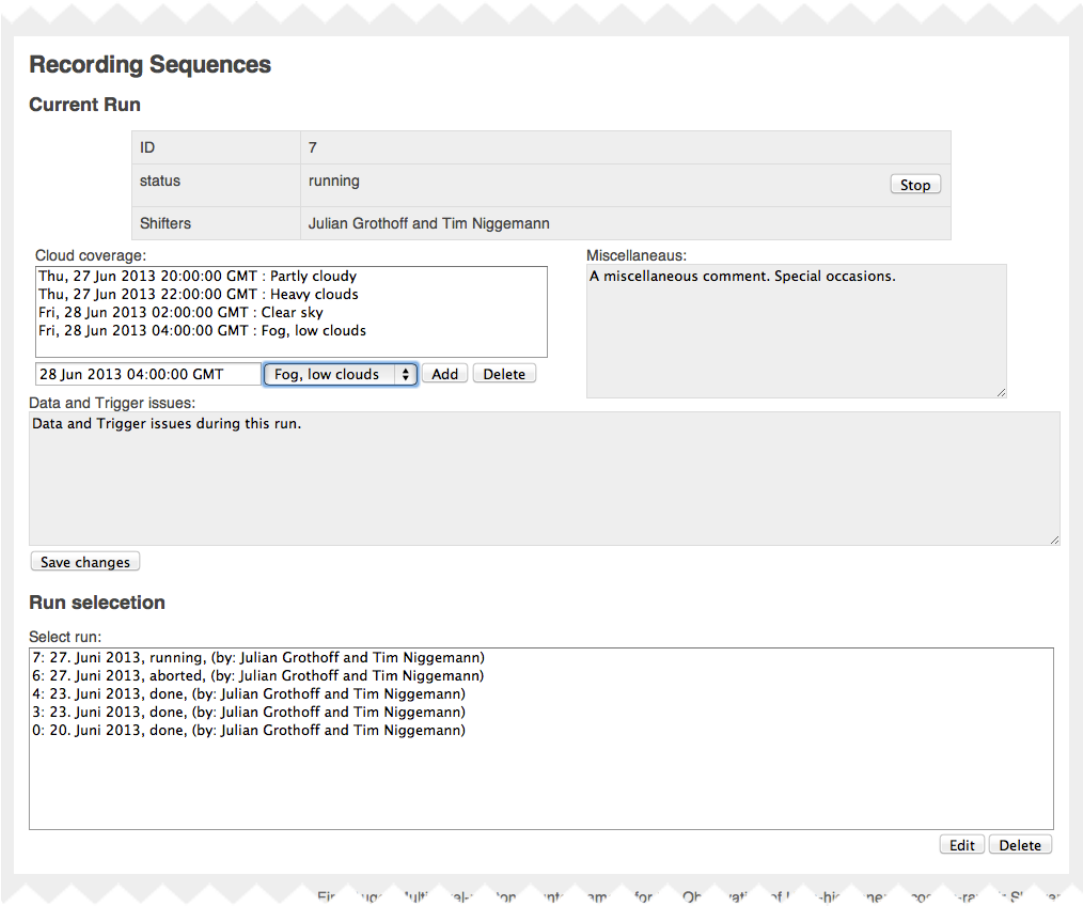

Figure 4.1.5: Screenshot of the "Run" page from FAMOUS webinterface.

the bias script is displayed confirming the settings and displaying the temperature and the adjusted bias-voltages. This step is useful to check single pixels with an oscilloscope and for a fine tuning of the bias-voltages.

- As described in section 2.2.4 the over-voltage of all SiPMs has to be calibrated. This step is explained in detail in the next section and the corresponding screenshot is found in figure 4.2.2.

- The last page starts the measurement process. Before that the desired over-voltage for all SiPMs can be entered and is calculated from the calibrated breakdown voltage. Here miscellaneous comments can be stored referring to the startup or details of this shift. On the start, the run with its data obtained from the preceding steps is stored in the "runs" collection of "famous" database, so that recorded events can be assigned to the current run.

The screenshot in figure 4.1.5 shows the "Run" page, when a run is in progress. If the page is loaded and a run is in duty it is automatically fetched from MongoDB and opened in the editing area at the top. The cloud-coverage at different times can be added, edited and deleted. Two fields for comments, one for the data and trigger issues, the other one for various comments, are given to document important findings during a run. To edit or delete older runs a selection for all runs in the picked time range is

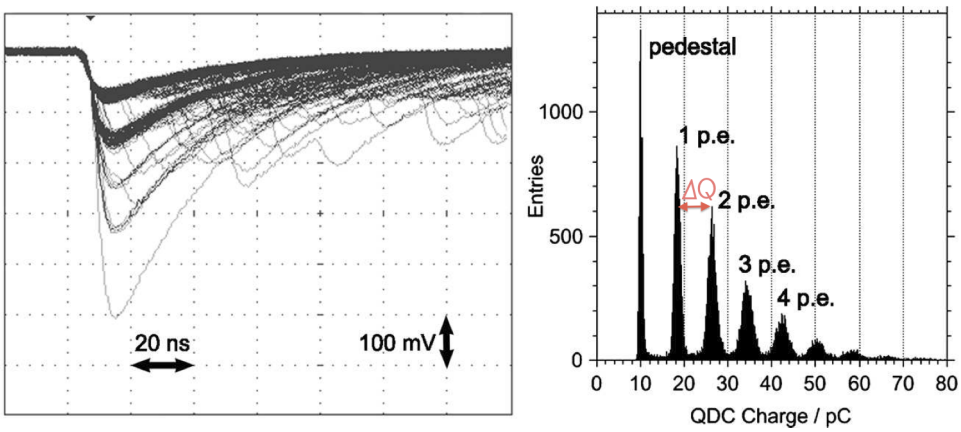

Figure 4.2.1: Measurements of an SiPM in a light-tight box and with a pulsed UV diode taken from [25]. *Left:* Typical oscilloscope image of an amplified noise signal. The number of coincidentally triggered cells is clearly distinguishable by the signal depths. *Right:* Finger-spectrum in SiPM charge measurement with clear peaks related to the number of cell breakdowns (p.e. = photon equivalent).

found at the bottom of the page. The current run can also be stopped from a button initializing the stop procedure. It is similar to the start procedure in reverse order. At first the shifters, start and end-time are checked and the data taking script is stopped. Then the overvoltage is calibrated again and a spectrum with bias-voltage off is taken, so that a comparison to the start values is possible and a stable run can be verified.

4.2 Breakdown-Voltage Calibration

As each cell of an SiPM has a p-n-junction with the applied bias-voltage V_{Bias} in reverse direction, the breakdown voltages (cf. section 2.2.4) vary with temperature. The Gain(G) of the geiger mode avalanche-photodiodes is proportional to the overvoltage, with an effective capacity of the SiPM and amplifier.

$$G = \frac{Q}{e} \propto V_{\mathrm{OV}}(T) = V_{\mathrm{Bias}} - V_{\mathrm{Break}}(T) \tag{4.2.1}$$

For this reason the bias-voltage has to be temperature adjusted for a stable overvoltage V_{OV} resulting in a stable gain. Moreover, the overvoltage determines the most of the SiPM characteristics in combination with the temperature (cf. figure 2.2.4). So the goal of the calibration is to find the breakdown voltage at a certain temperature in order to have a good temperature adjustment for the gain (For details see chapter 6.3 in [17]) and to set the same overvoltage for each SiPM. To set the bias-voltage at 25 °C,

the measured breakdown-voltage at a certain temperature T can be transformed using the temperature progression coefficient $\beta = 56\,\mathrm{mVK}^{-}1$.

$$V_{\mathrm{Bias}}(25\,^{\circ}\mathrm{C}) = V_{\mathrm{OV}} + V_{\mathrm{Break}}(25\,^{\circ}\mathrm{C}) = V_{\mathrm{OV}} + V_{\mathrm{Break}}(T) + \beta \cdot (25\,^{\circ}\mathrm{C} - T) \qquad (4.2.2)$$

Scripts from the SiPM library developed at RWTH Aachen already have functions for breakdown analysis and the used module (FTPC) for operating the bias-voltage supports the use of the temperature progression efficient.

A typical SiPM Oscilloscope reading is shown in figure 4.2.1. The signal depth of the oscilloscope readout is quantised in the count of simultaneous triggered cells, which is clearly distinguishable. This can also be seen in the integrated charge spectrum next to the oscilloscope image as photon equivalent (p.e.) charges. For the extrapolation of the breakdown voltage the gain needs to be plotted against the bias-voltage. As the gain is a linear function of the bias-voltage a linear fit has to be done, so that the gain can be extrapolated down to zero. Therefore the charge difference ΔQ between one and two p.e. as shown in the QDC-spectrum in figure 4.2.1 can be fitted instead of the gain, because ΔQ is proportional to it. A peakfinder is applied to find the maxima in the finger-spectrum, so that the error on this fit combined with the QDC resolution is given as input errors for the linear regression.

4.2.1 Calibration Step in FAMOUS Webinterface

These Calibrations are done in the 4th step of a new run procedure and during the stop-procedure as well. Therefore the predefined bias-voltage values are diversified in a specific range depending on the calibration type select (Fast/Slow Calibration). When a calibration is started, the various bias-voltages are set and each time a QDC-spectrum is taken. Afterwards for each pixel and bias-voltage the first two peaks are estimated with the ROOT TSpectrum peakfinder algorithm and the linear regression as described above is done by a script. Then the calibration is stored in a calibration collection of the famous database with a sequential number.

Hence the calibration is selectable during the new run procedure as shown with example data in figure 4.1.1. In a camera view, which is the same as in the eventdisplay (see next sequence), each SiPM is selectable and the calculated data from the linear regression for each is presented in a tooltip. By the click on a certain pixel the linear fit is shown beneath the camera view. In the bottom a text field can be used to note comments on the done calibrations and causes for the selection of the calibration, which is used for the over-voltages later.

In the last step of the new run sequence the common overvoltage for all SiPMs can be entered. Then the corresponding bias-voltage for each pixel is calculated from the breakdownvoltages of the selected calibration. This voltage is set on every pixel when the measurement is started.

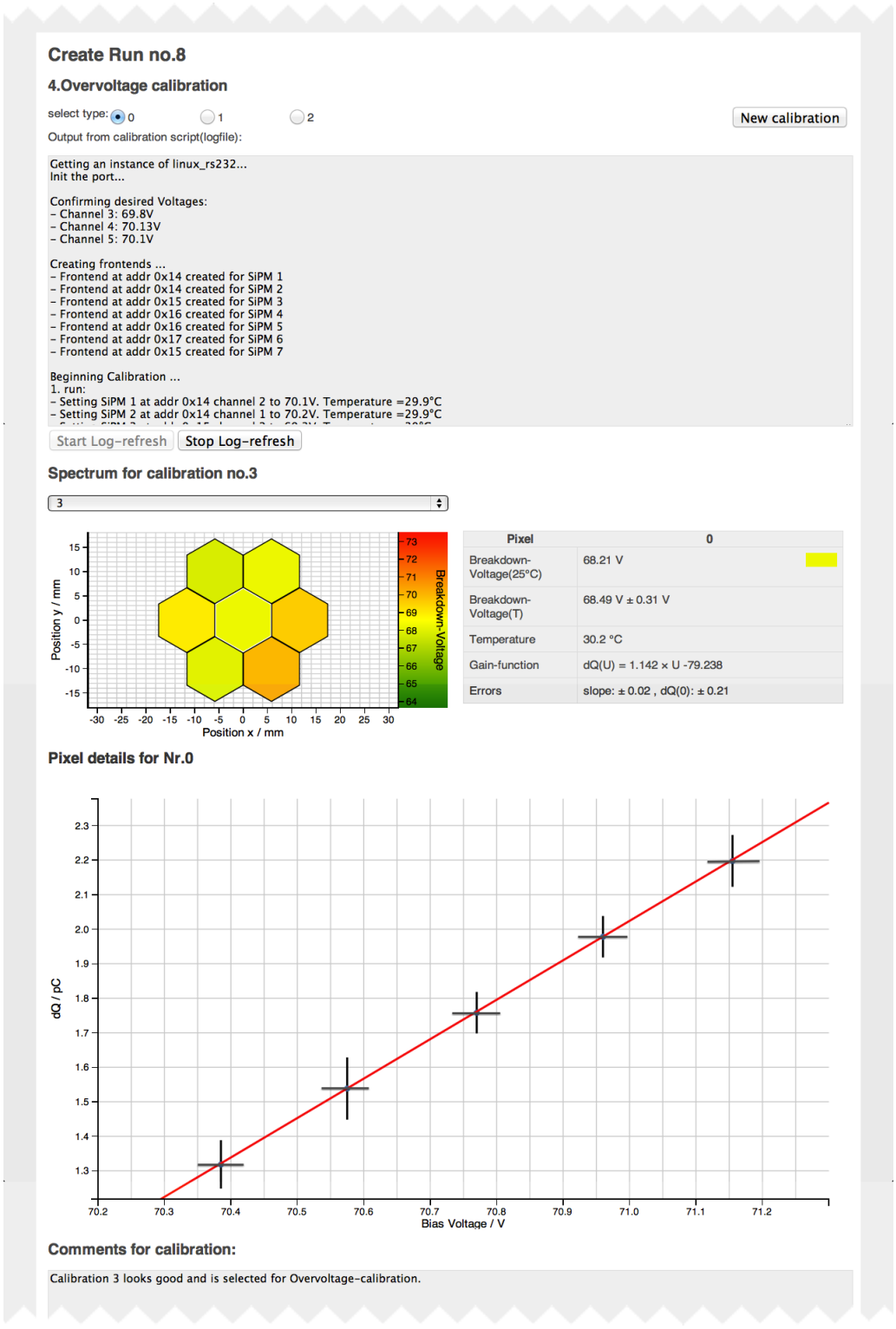

Figure 4.2.2: Screenshot of the fourth step of the start sequence, containing the breakdown-voltage calibration.

4.3 Event Recording

Later during real measurements a cosmic ray event is triggered and recorded afterwards. An event has always an exact timestamp from the GPS-synced time and an continuous event number. For all pixel fired during one event a QDC spectrum has to be taken for the analysis. Furthermore, the timing relative to the first triggered SiPM is important to reconstruct the light path. For the evaluation of overvoltage values for example the current temperature and bias-voltage has to be stored in the event entry as well.

For test purposes, only minimum bias data is recorded periodical during a run, which is described in section 4.5. In the futre an appropriate trigger can easily replace the time controlled data taking. In order to set up a simple event display as described in the next chapter the mean QDC channel is calculated for each pixel right before the storage in the database.

4.4 Event Display

The "Eventdisplay" page on the FAMOUS webinterface has a selection for completed and running shifts. A screenshot of the page with fictitious data is shown in figure 4.4.1.The selection contains runs in specified time range at the top menu only. If such a run sequence is selected some basic information like an continuos number, the status, the shifters, start-time, end-time, moon fraction, cloud coverage at specific times, the bias-voltage at start and different comments are shown. Moreover, the number of events in this run is given and the events of this shift can be selected by their unique continuous number.

A selected event is loaded from the MongoDB and occurs in the 7 pixel camera view beneath. The hexagonal pixels are in the correct scale in x- and y-dimensions and each pixel can be picked constantly with a full QDC-spectrum by click or dynamically with a tooltip by mouse over. These functions, written in javascript, are coded to be easily extended to 64 pixels. For first evaluation the mean QDC channel is color coded in the chart. If a pixel has no data it is displayed white. Later a triggered event should be identifiable as a track in the camera view. The tooltip shows the mean QDC-channel value of the event and of the calibration measurement with bias off. The current bias-voltage, bias temperature and the x-/y-position in mm are revealed as well. If a pixel is selected by click the full QDC-spectrum is plotted as histogram together with its mean value. The details of the triggered events will help to ascertain real cosmic ray events and determine the quality of the triggered measurement.

4.5 Test Run

To proof the working principle of the calibration measurement and to show the stable operation of the SiPMs a test run with minimum bias data was done.

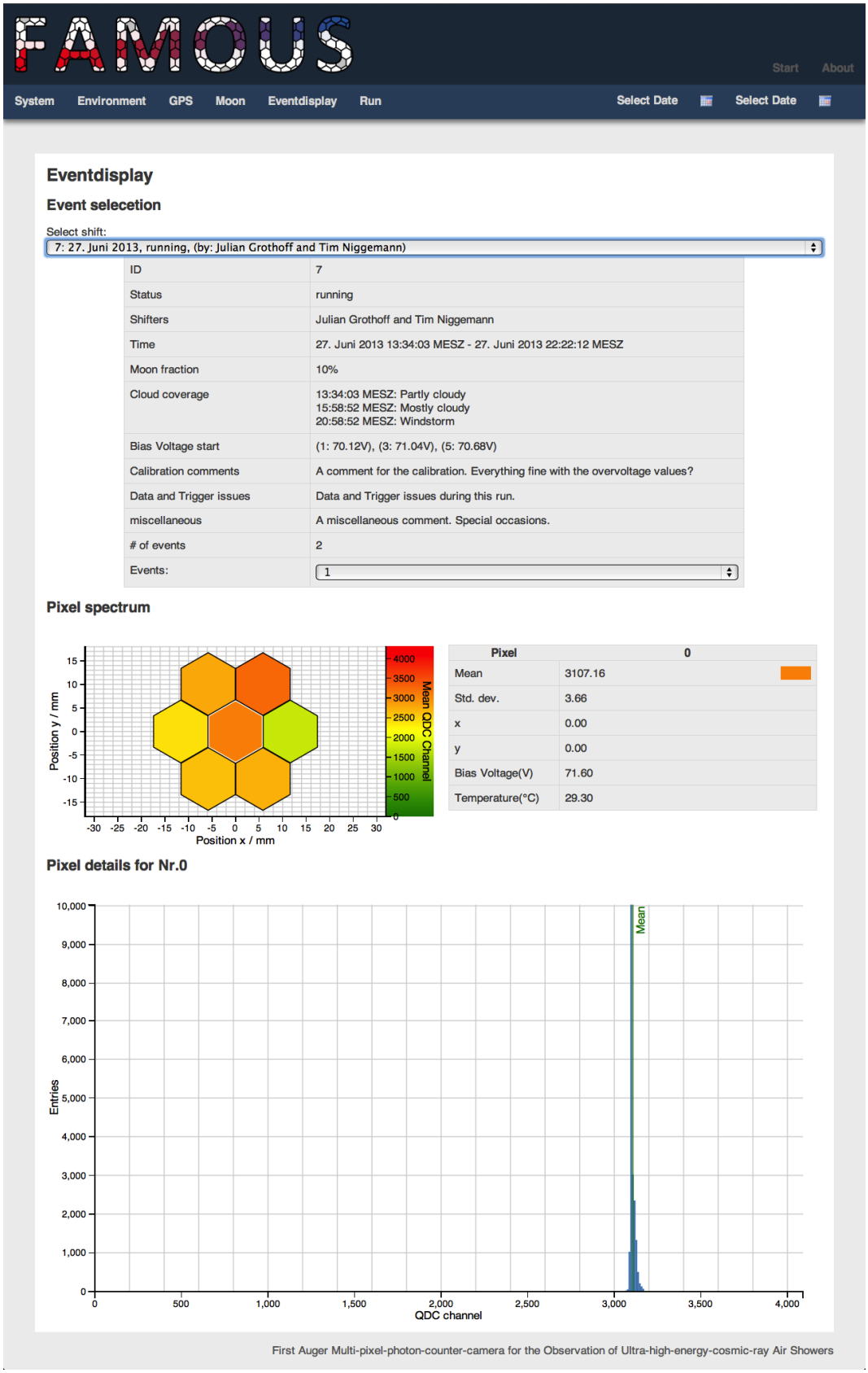

Figure 4.4.1: Screenshots of the "Eventdisplay" page from FAMOUS webinterface with example data.

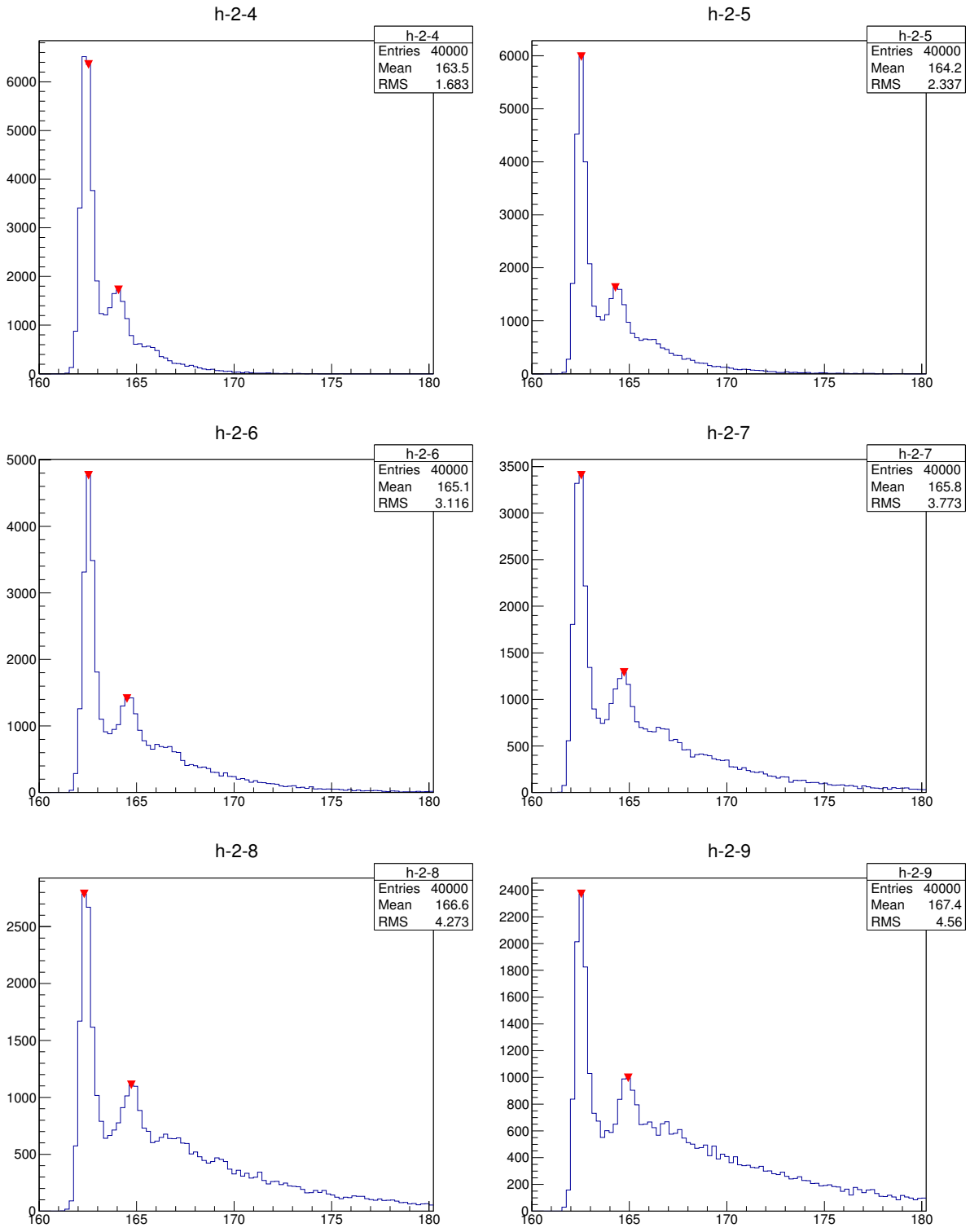

Figure 4.5.1: Example QDC-spectra for breakdown-voltage calibration of SiPM no. 2

Bias-Voltage [V]	70.575	70.77	70.96	71.155	71.345	71.54
ΔQ [pC]	1.32	1.54	1.76	1.98	2.20	2.42

SiPM no.	0	1	2	3	4	5	6
V_{break} [V]	68.11	69.76	69.42	69.09	70.13	70.19	69.28
$\pm\sigma_{V_{\text{break}}}$	$\pm$0.33	$\pm$0.28	$\pm$0.28	$\pm$0.23	$\pm$0.25	$\pm$0.45	$\pm$0.27
Temperature [°C]	31.2	31.0	31.0	31.2	31.6	31.6	30.9
χ^2 /ndf	1.3	0.4	0.0001	0.7	0.7	0.0001	0.5
V_{bias} (25 °C) [V]	69.07	69.73	70.39	70.04	71.06	71.12	70.25

Table 4.5.1: *Top*: Obtained data for the calibation of pixel no. 2 (at 31 °C SiPM temperature). Bottom: Fit results and calculated bias-voltages for an over-voltage of 1.3V.

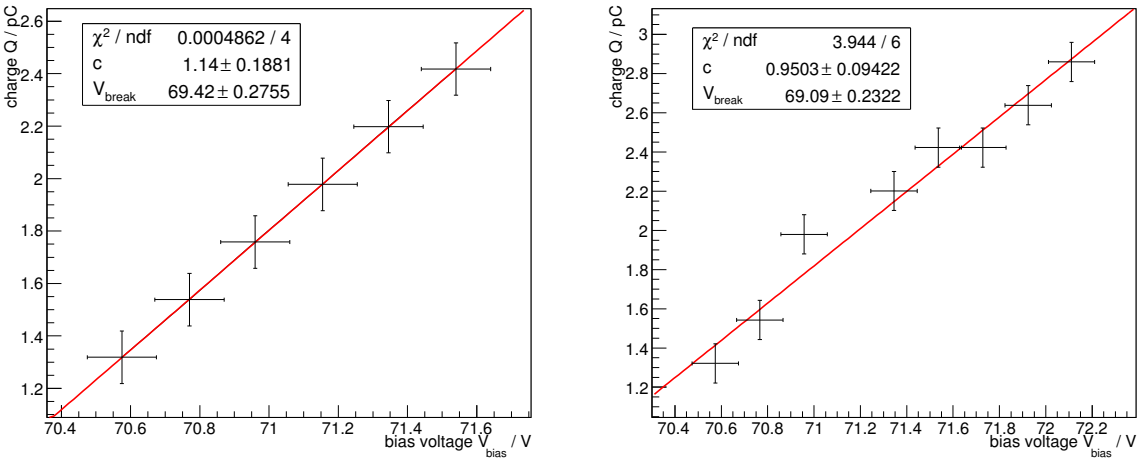

Figure 4.5.2: Linear regression for the breakdown-voltage extrapolation for pixel no. 2 (*left*) and 3 (*right*).

4.5.1 Calibration

Therefore the breakdown-voltage calibration measurments were done with C++ and ROOT. In figure 4.5.1 the measured QDC spectra with two photon equivalent peaks, found by the ROOT TSpectrum peakfinder, during the variation of the bias-voltage are presented. For the so-called fingerspectrums always one of the four single SiPMs of each pixel is connected aditionally to the sum signal and read out with the QDC. The Bias voltage was set to the same certain values in a voltage range for each pixel. After that, the Linear regression as described in the calibration section is shown for pixel 2 with a very good fit and for pixel 3 in figure 4.5.2. The obtained ΔQ values for pixel number two are presented in table 4.5.1 together with the fit results for all pixel. Plots for all linear regressions can be found in the appendix. As each pixel has an individual breakdown-voltage, the choosen voltage range for the bias-voltage could be changed to a regime suitable for the current SiPM in the future. Thus saturation effects of the gain at higher voltages do not set in for models with low breakdown voltage. Moreover, the peakfinder and its parameters could be modified for better results.

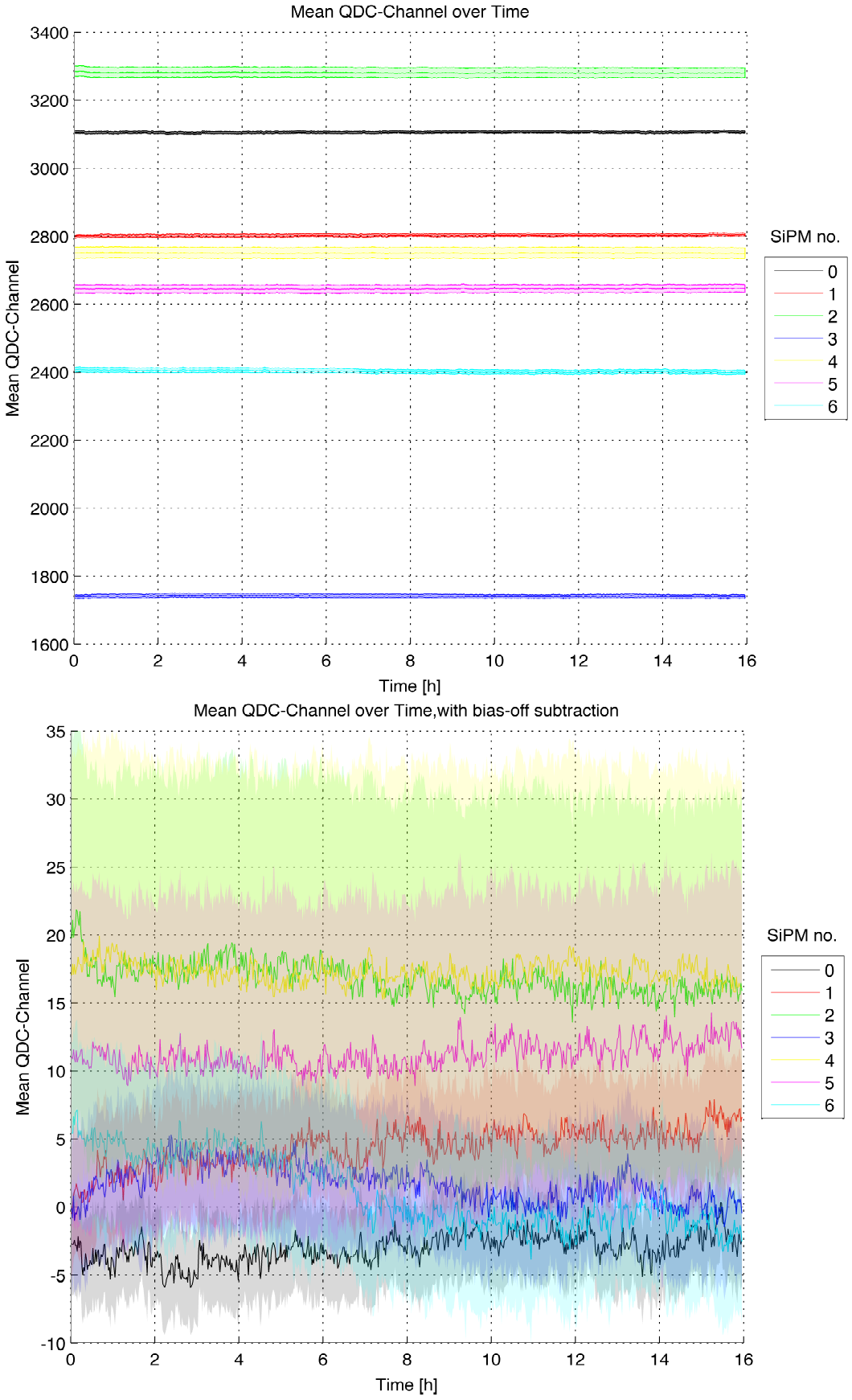

Figure 4.5.3: QDC spectrum of all 7 pixel without (*top*) and with (*bottom*) mean bias-off subtraction. The error range is given in the transparent color of the corresponding line.

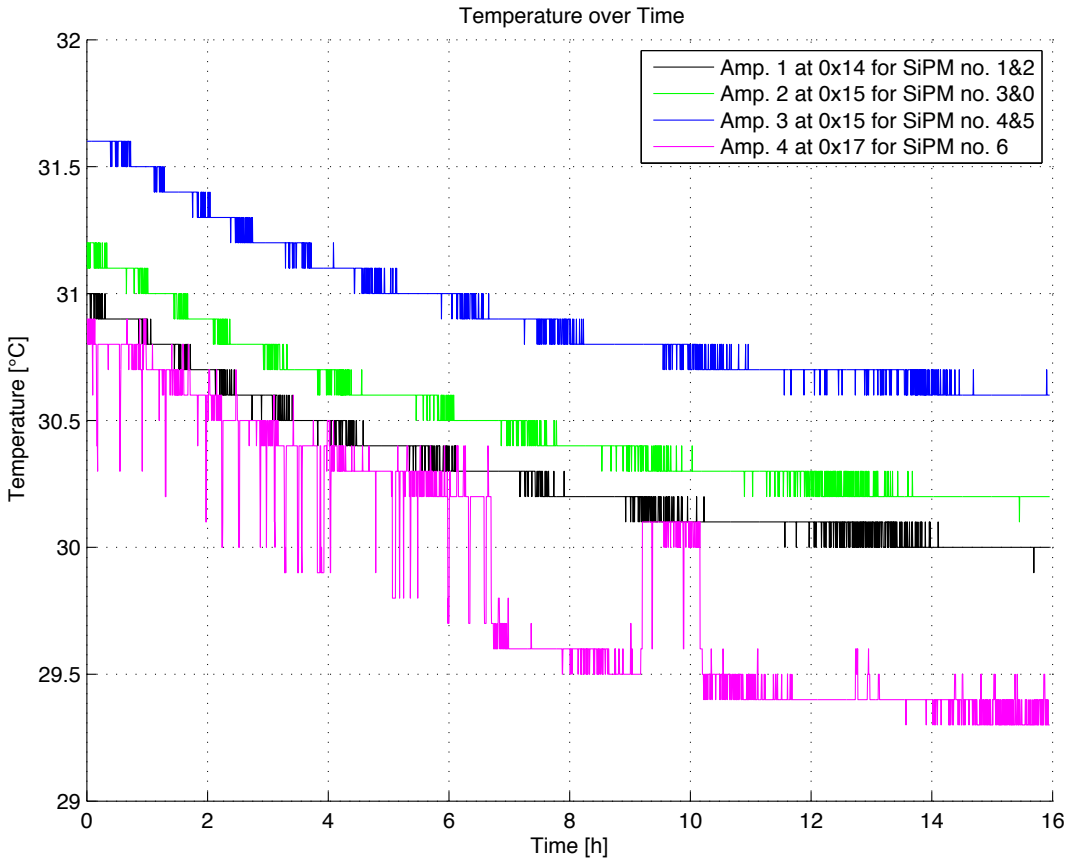

Figure 4.5.4: Temperature time traces during measurment for all 4 amplifiers.

4.5.2 Minimum Bias Data Measurement

As the fits show good results for the breakdown-voltage calibration, the calculated bias-voltages have been set and a measurement over approx 16 hours in the dark has been done. Therefore a Overvoltage of 1.3V was choosen as compromise between noise effects and a high PDE and as it will probably used later. To trigger the QDC the pulser of the Wiener VM-USB interface with 200ns pulsewidth and 50 kHz frequency was connected to the QDC. During the startup some SiPMs signals were watched on a oscilloscope. In doing so a small interference signal was observed on the oscilloscope each time the QDC is triggered. The source of the singal could not be specified, although even another pulser was tried. Another issue is the different baseline of the SiPMs, which leads to different mean QDC values, because of the integrated SiPM current flow.

Like in the run sequence of the FAMOUS webinterface a QDC spectrum with bias-voltage off has been taken before, referred to as bias-off spectrum, and after the measurment. During the run approx every minute a QDC spectrum with about 500,000 entries was taken so that 729 spetra were recorded. Afterwards the mean and root-mean-square value of each sum-signal from the Fan-In/Out for every pixel has been calculated. In the following the SiPM number stands for the sum signal of each pixel, where SiPM number zero is in the middle and the 6 other pixels are arranged clockwise.

Amplifier no.	SiPM no.	Slope [QDC chan./h]	Offset [QDC chan.]	χ^2/ndf
1	1	0.25 ± 0.04	2.4 ± 0.3	0.04
1	2	-0.16 ± 0.11	10.8 ± 1.1	0.004
2	0	0.12 ± 0.03	-4.0 ± 0.3	0.06
2	3	-0.18 ± 0.04	3.2 ± 0.4	0.04
3	4	-0.03 ± 0.12	17.5 ± 1.2	0.003
3	5	0.11 ± 0.09	10.3 ± 0.9	0.005
4	6	-0.47 ± 0.05	4.9 ± 0.5	0.04

SiPM no.	0	1	2	3	4	5	6
Bias-off before	3106.4	2798.1	3264.4	1741.7	2733.3	2633.1	2403.7
standard deviation	±3.4	±2.6	±2.7	±3.6	±4.3	±2.9	±2.9
Bias-off after	3108.1	2800.3	3264.8	1738.8	2733.4	2634.2	2400.9
standard deviation	±3.6	±2.9	±3.1	±4.0	±4.7	±4.3	±3.1
difference	1.7	2.2	0.4	- 2.9	0.1	1.1	2.8

Table 4.5.2: *Top*: Fit results of linear regressions for each SiPM mean QDC value. *Bottom*: Mean QDC channels and root-mean-squre values from bias-off spectrum, taken before and after the measurement.

4.5.3 Minimum Bias Data Analysis

The time trace of the mean QDC values and their errors are shown in figure 4.5.3. The plot indicates, that the mean value is constant which was expected for a good calibration and temperature adjustment of the bias-voltage. In the second plot the mean of the bias-off spectrum was subtracted for each pixel. Thus the lines moved together as expected, reducing the effect of the different baselines of the SiPMs. Hence, all time traces of the mean QDC spectrum are in the range of their errors comparable and have a similar QDC mean value, if the bias-voltage is set and adjusted correctly. The bias-off spectra before and after the run are very compatible as the values of the second measurement after 16 hours is within the error range of the first measurement, which can be seen in table 4.5.2. In conclusion the bias-off mean QDC value is nearly constant over time and thus the baseline level of the SiPMs is stable. Conspicuous is, that the bias-off value from pixel number zero is below the measured values with bias-voltage turned on, so that after the subtraction of the mean bias-off value the corrected value is below zero. In prospective measurements it could be proficient to subtract the whole spectrum from each QDC spectrum and build the mean afterwards.

To analyse the stability of the mean QDC value the temperature of each of the 4 double channel amplifiers build into FAMOUS[7] has been taken during the measurement. Figure 4.5.4 shows that over night the temperature went down approx 1 °C at all four amplifiers. A linear regression for each SiPM mean QDC charge has been done and is presented in figure 4.5.5 separated to each amp. In the appendix the regression for each pixel alone with its residuals can be found. The fit results are shown in table 4.5.2. All fitted lines are wide within the error range, so that the χ^2/ndf values are very low. This relative high noise may correspond to the high noise of the baseline seen on the oscilloscope. It could be reduced in future by the use of slower operational amplifier for the FAMOUS Fan-Out module, which would introduce less baseline noise

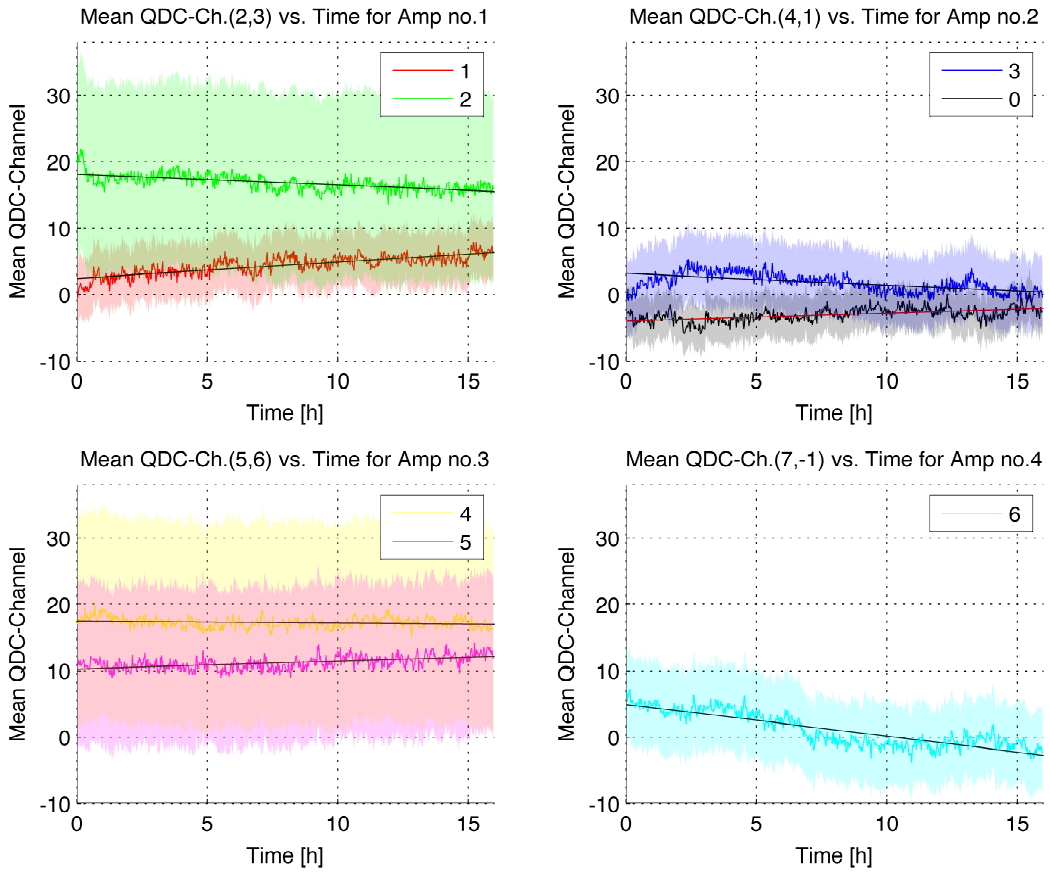

Figure 4.5.5: QDC mean value of the SiPMs connected to each of the four double channel amplifiers build into FAMOUS[7]. For each mean QDC time trace a linear regression has been done.

compared to the current model. The falling drift of the bias temperature is not seen in the regressions, so that a good temperature adjustment of the FTPC hardware is done and all QDC mean values are stable enough to perform cosmic ray experiments. The worst observed drift is -0.47 QDC channels per hour. For every amplifier except the fourth a rising and a falling trend can be observed in the mean QDC time trace. This is a hint, that the temperature progression efficient, which was the same for all SiPMs ($\beta = 56\,\mathrm{mVK}^{-}1$), is a good average value. A single calibrated temperature progression coefficient for each SiPM may lead to better results.

5 Summary and Outlook

The research with the "First Auger Multi-photon-pixel-counter-camera for the Observation of Ultra-high-energy cosmic ray air Showers" is a challenging topic, offering great advantages for a improved understanding of cosmic rays.

As presented in the beginning, FAMOUS[7], the seven pixel fluorescence telescope based on SiPMs, is almost ready for first measurement shifts. The developed Data Acquisition System in this thesis was set up from a Raspberry Pi mini computer, running a responsible Apache webserver and a highly capable MongoDb database. On this webserver the webinterface was programmed, which is able to control the operational telescope prototype, acquire the data from it and present it on simple webpages after storing it in the database. Moreover, an Arduino microcontroller electronic board was programmed and populated with sensors for GPS, light, temperature, pressure and humidity to obtain environmental data. For this environment unit a custom designed box was planned and then manufactured in-house. Noise measurements of the sensors and tests of the chosen hardware components and software has proofed, that the predetermined requirements are fulfilled. In connection with the environment unit, the DAQ already takes data and stores it in its database.

To research with FAMOUS a run sequence was elaborated and programmed into the webinterface. For a brief overview of prospective cosmic ray measurements, an eventdisplay was integrated in the webinterface. The run sequence also contains a breakdown-voltage calibration for the stable operation of FAMOUS[7] at desired over-voltages. The calibration and working principle of the run sequence was tested in a minimum bias data measurement, confirming the stability of the mean QDC value. Although the results for minimum bias data were compatible with the expectations, some possible improvements were marked in this research.

In conclusion the goal to assemble an operational DAQ from a mini computer for FAMOUS with an environment sensor system based on a microcontroller has been achieved. Moreover, an adequate webinterface for control and data read out was installed. Finally a test run has confirmed the elaborated recording sequence.

This thesis has shown the possible applications of a mini computer as a DAQ. Due to further progress like the use of a mini computer with higher performance, these applications could be expanded. A gyroscope sensor could be mounted at the telescope and connected to the Arduino board to log the telescopes angular position for example. Basically more test runs with the DAQ should be done for hints of further development, as the software based solution with the Raspberry Pi offers a high flexibility. A precise trigger for subsequent measurements will be build on a dedicated electronics board for the 64 pixel version of the telescope. The final test run has depicted different opportunities for improvements. At first the observed interference on the SiPM

signal during QDC measurements should be investigated and eliminated. Then the breakdown-voltage calibration can be improved by the determination of the gain in a bias-voltage regime suitable for the current SiPM and by enhanced peak finder technique. The measurement setup could be refined by the use of a low-noise operational amplifier for the FAMOUS Fan-Out module and by equalising the baseline offsets on all sum channels.

After all, FAMOUS[7] ,operated by the created DAQ in this thesis or a DAQ, which may benefit from this study, and its 64 pixel successor will measure its first cosmic rays in the near future.

Bibliography

[1] Collaboration A. Pierre auger observatory - cosmic rays. — URL: www.auger.org/cosmic_rays/ (online; accessed: 2013-07-20).

[2] Extensive cosmic-ray showers / Pierre Auger, P. Ehrenfest, R. Maze et al. // Rev. Mod. Phys. — 1939. — Jul. — Vol. 11. — P. 288–291. — URL: http://link.aps.org/doi/10.1103/RevModPhys.11.288.

[3] Famous: A prototype silicon-photomultiplier telescope for the fluorescence detection of ultra-high-energy cosmic rays / Markus Lauscher, Pedro Assis, Pedro Brogueira et al. // SPIE NanoScience+ Engineering / International Society for Optics and Photonics. — 2012. — P. 84601N–84601N.

[4] Hess V. F. Beobachtungen der durchdringenden strahlung: bei sieben Freiballonfahrten. — Kaiserlich-Königlichen Hof-und Staatsdruckerei, in kommission bei Alfred Hölder, 1912.

[5] Walter M. Ein höhenflug der physik // Physik Journal. — 2012. — Vol. 11, no. 6. — P. 53.

[6] whanlon@cosmic.utah.edu. Cosmic ray spectra of various experiments. — URL: http://www.physics.utah.edu/~whanlon/spectrum.html.

[7] Fermi E. On the origin of the cosmic radiation // Phys. Rev. — 1949. — Apr. — Vol. 75. — P. 1169–1174. — URL: http://link.aps.org/doi/10.1103/PhysRev.75.1169.

[8] Collaboration P. A. Breakthrough in cosmic ray mystery - possible sources found for high energy particles that bombard the earth. — 2007. — Nov. — P. 2. — URL: http://www.auger.org/news/PRagn/releases/rel99_STFC_JM_UK.html.

[9] Blümer J., Engel R., Hörandel J. R. Cosmic rays from the knee to the highest energies // Progress in Particle and Nuclear Physics. — 2009. — Vol. 63, no. 2. — P. 293–338.

[10] Obermeier A. The fluorescence yield of air excited by electrons measured with the AIRFLY experiment. — Forschungszentrum Karlsruhe in der Helmholtz-Gemeinschaft, 2007.

[11] The fluorescence detector of the pierre auger observatory / J Abraham, P Abreu, M Aglietta et al. // Nuclear Instruments and Methods in Physics Research Section A: Accelerators, Spectrometers, Detectors and Associated Equipment. — 2010. — Vol. 620, no. 2. — P. 227–251.

[12] Auger: Zukunft. — URL: `http://www.auger.de/public/zukunft.html`.

[13] Niggemann T. New Telescope Design with Silicon Photomultipliers for Fluorescence Light Detection of Extensive Air Showers : Ph. D. thesis / Tim Niggemann ; Master's thesis, III. Phys. Inst. A, RWTH Aachen University, Aachen, Germany. — 2012.

[14] Musienko Y. State of the art in SiPM's. — 2011. — Feb. — CERN, SiPM workshop, 16.02.2011. URL: `https://indico.cern.ch/getFile.py/access?contribId=11&sessionId=7&resId=0&materialId=slides&confId=117424`.

[15] Rennefeld J., Stahl A. Studien zur eignung von silizium photomultipliern f* ur den einsatz im erweiterten cms detektor am slhc : Ph. D. thesis / Jörg Rennefeld, A Stahl ; Diplomarbeit. — 2010.

[16] Status of the silicon photomultiplier telescope famous for the fluorescence detection of uhecrs / TIM NIGGEMANN, PEDRO ASSIS, PEDRO BROGUEIRA et al. // dep. — Vol. 3. — P. d2Nγ.

[17] Lauscher M. Characterisation studies of silicon photomultipliers for the detection of fluorescence light from extensive air showers. — 2012. — Jan.

[18] The uv sensitivity improvement of mppc / K Sato, K Yamamura, T Nagano et al. // Nuclear Instruments and Methods in Physics Research Section A: Accelerators, Spectrometers, Detectors and Associated Equipment. — 2013.

[19] Nitz D. Triggering and data acquisition systems for the auger observatory // Nuclear Science, IEEE Transactions on. — 1998. — Vol. 45, no. 4. — P. 1824–1829.

[20] Corporation G. T. Product user manual gps receiver engine board product user manual gps receiver engine board em-406a. — URL: `https://www.sparkfun.com/datasheets/GPS/EM-406A_User_Manual.PDF` (online; accessed: 10.06.13).

[21] Solutions T. A. O. Tsl2560, tsl2561 light-to-digital converter. — URL: `http://www.adafruit.com/datasheets/TSL2561.pdf` (online; accessed: 10.06.13).

[22] GmbH B. S. Bmp085 digital, barometric pressure sensor. — URL: `https://www.sparkfun.com/datasheets/Components/General/BMP085_Flyer_Rev.0.2_March2008.pdf` (online; accessed: 10.06.13).

[23] Inc. H. I. Hih-4030/31 series - humidity sensors. — URL: `https://www.sparkfun.com/datasheets/Sensors/Weather/SEN-09569-HIH-4030-datasheet.pdf` (online; accessed: 10.06.13).

[24] mongodb. — URL: `http://www.mongodb.org` (online; accessed: 15.06.13).

[25] Future use of silicon photomultipliers for the fluorescence detection of ultra-high-energy cosmic rays / Maurice Stephan, Thomas Hebbeker, Markus Lauscher et al. // SPIE Optical Engineering+ Applications / International Society for Optics and Photonics. — 2011. — P. 81551B–81551B.

List of Figures

Appendix

Time Traces for Noise Measurements of Arduino Sensors

All measurements have been done in 30s with a maximum refreshrate of the Sensors.

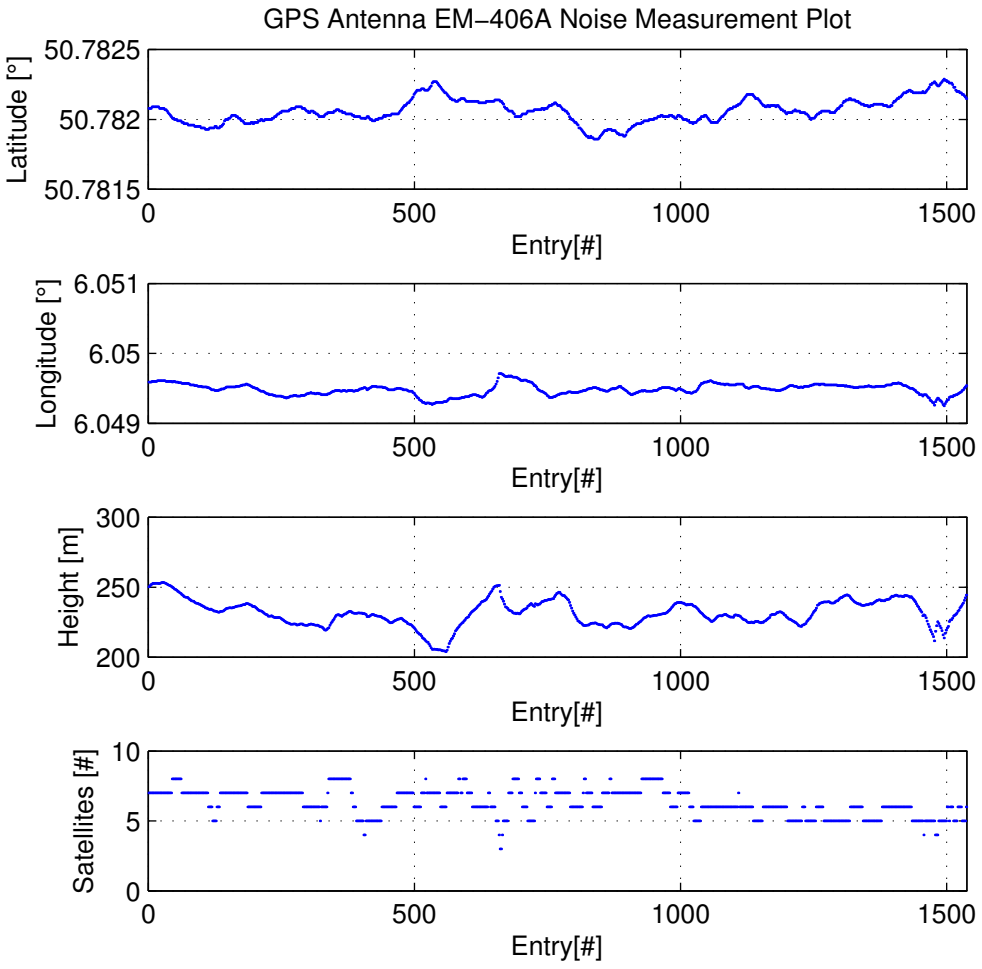

Figure 5.0.1: GPS-receiver noise measurement.

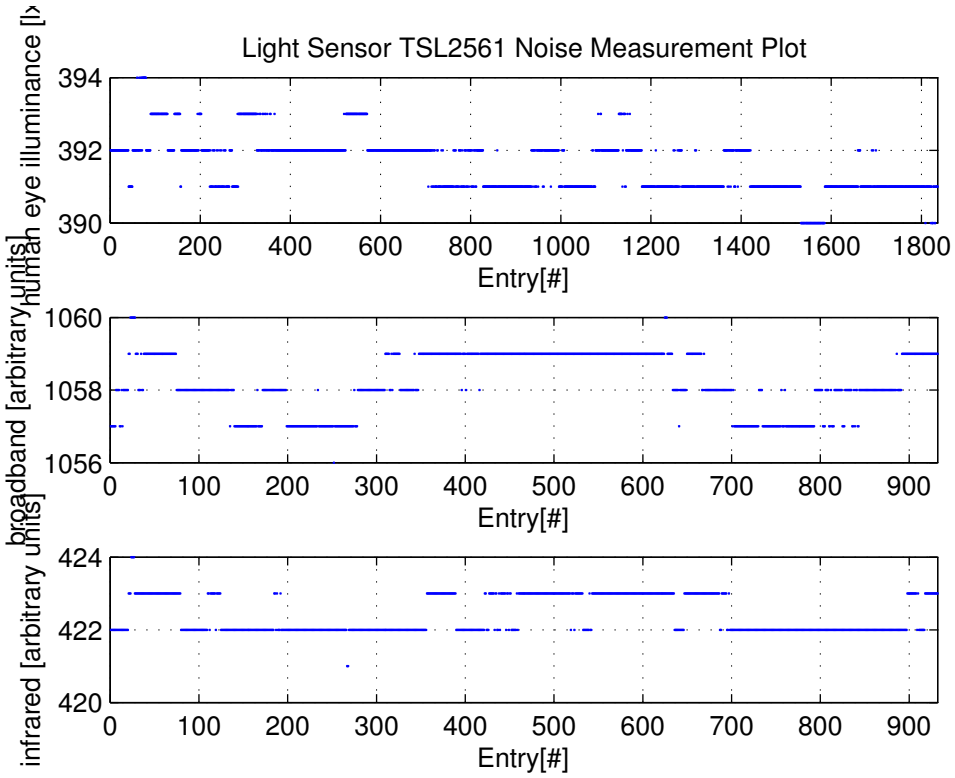

Figure 5.0.2: Light sensor noise measurment.

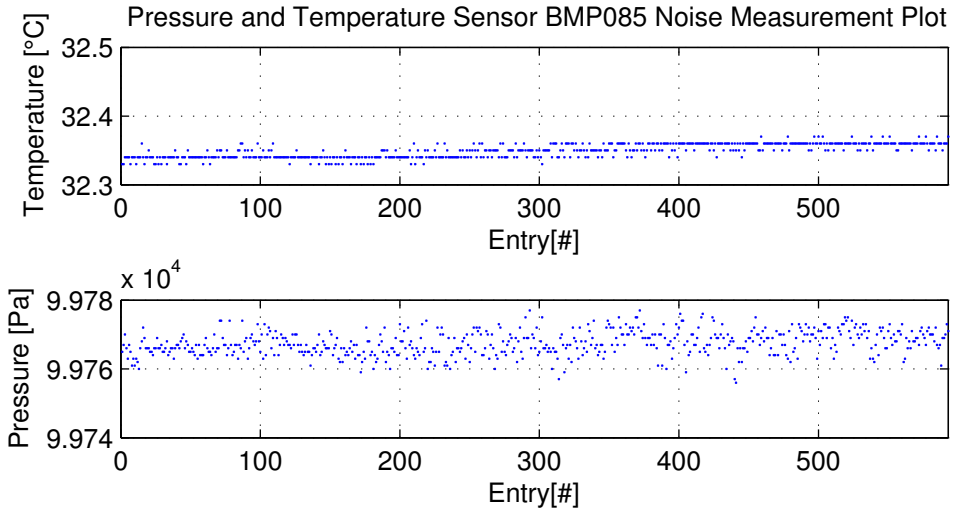

Figure 5.0.3: Combined pressure and temperature sensor noise measurement.

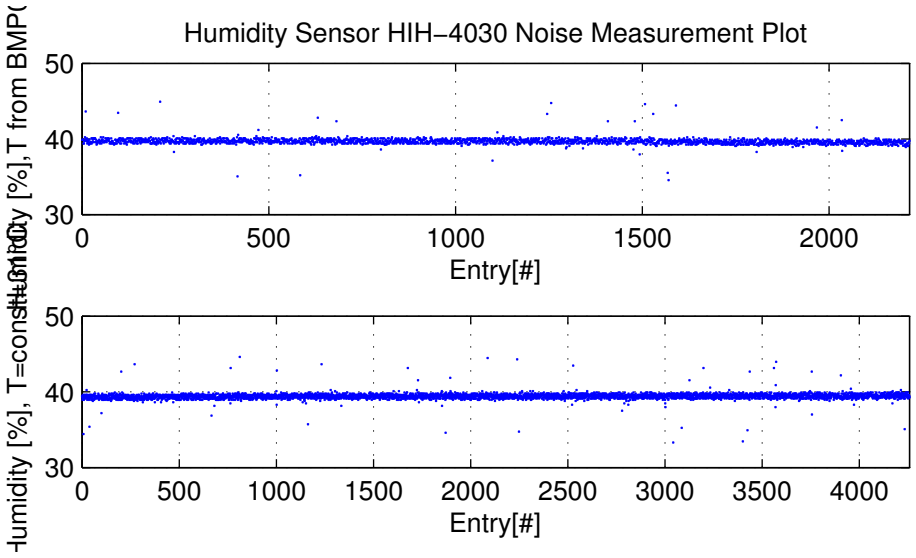

Figure 5.0.4: Humidity sensor measurement.

Breakdown-Voltage Calibration Fits

The fit results are shown in table 4.5.1.

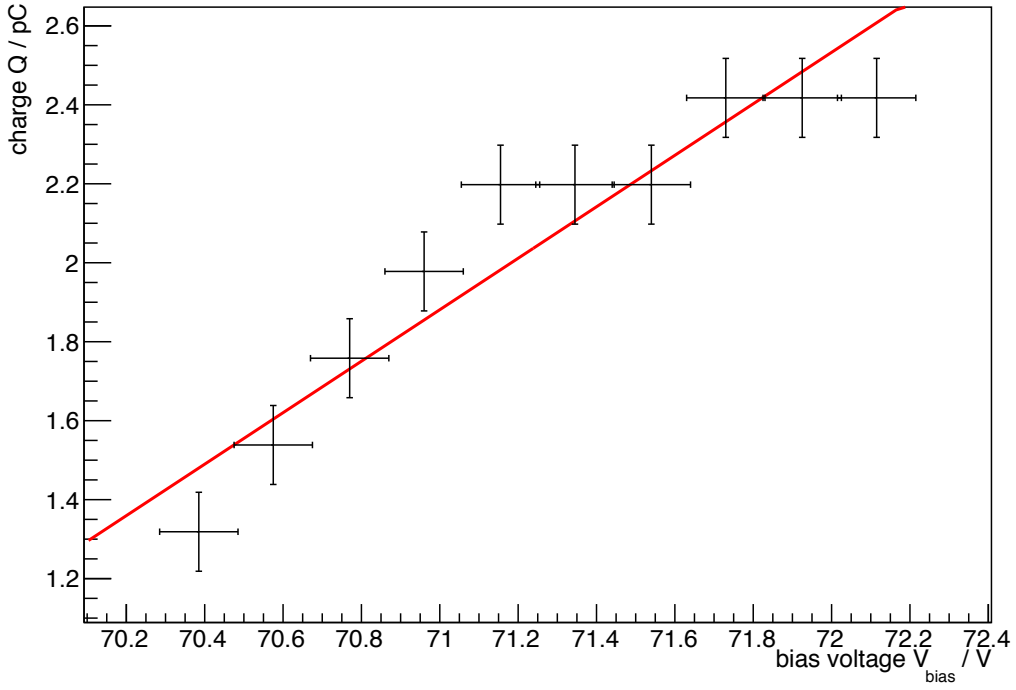

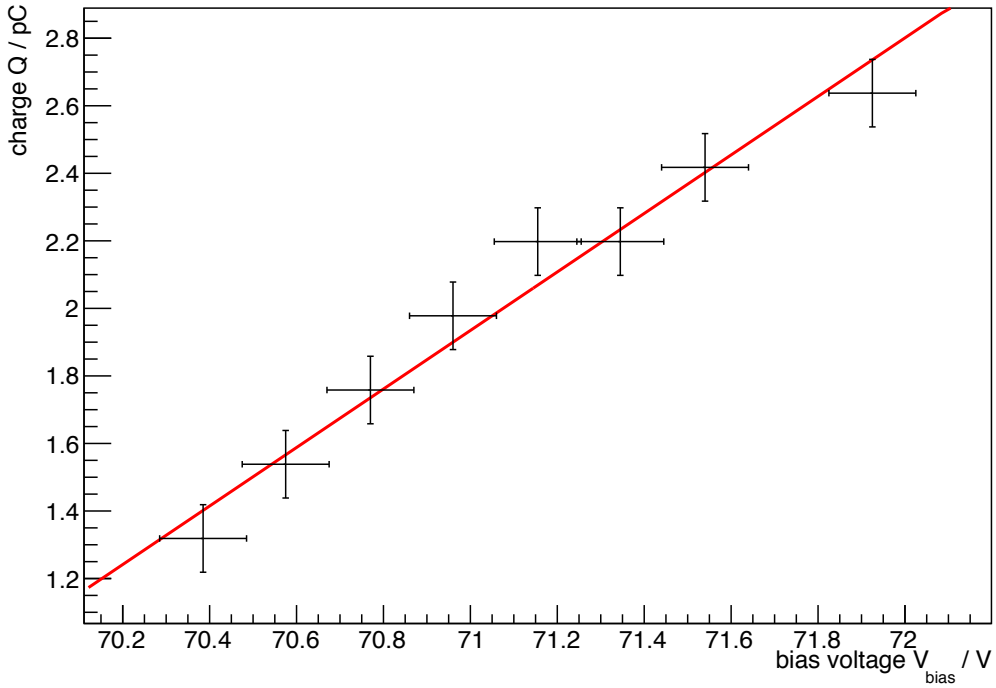

Figure 5.0.5: Breakdown-voltage calibration for SiPM no. 0 and 1.

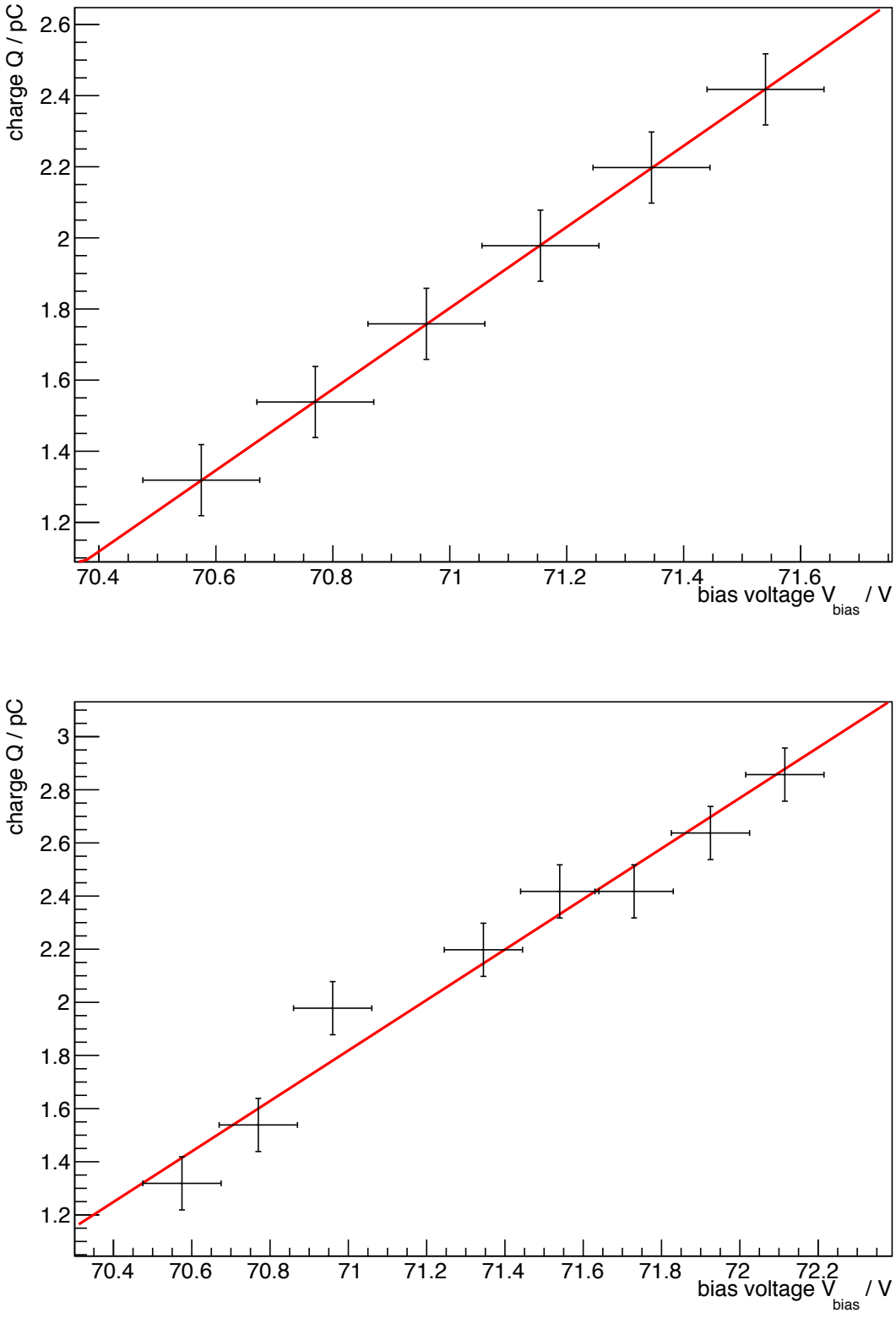

Figure 5.0.6: Breakdown-voltage calibration for SiPM no. 2 and 3.

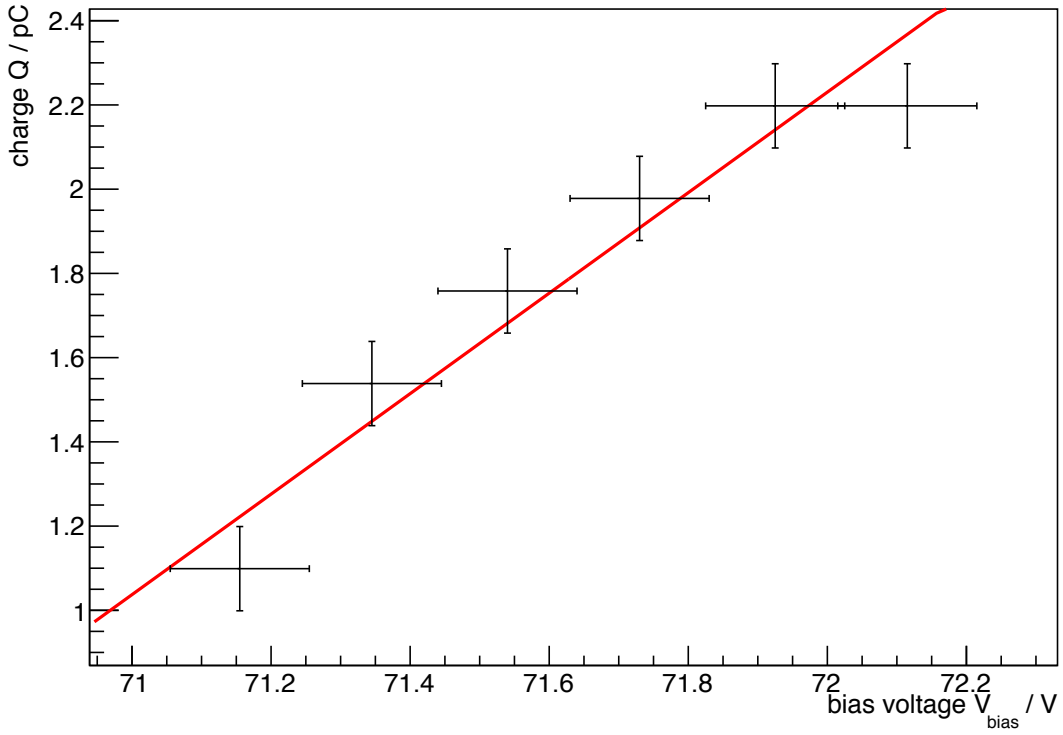

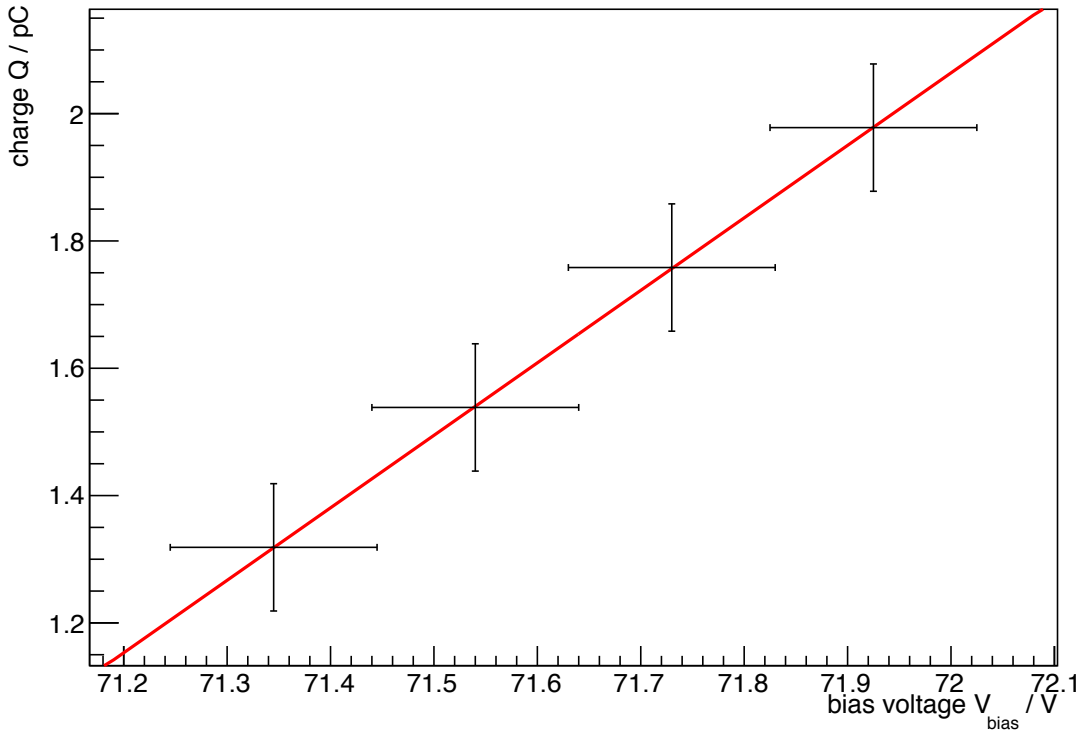

Figure 5.0.7: Breakdown-voltage calibration for SiPM no. 4 and 5.

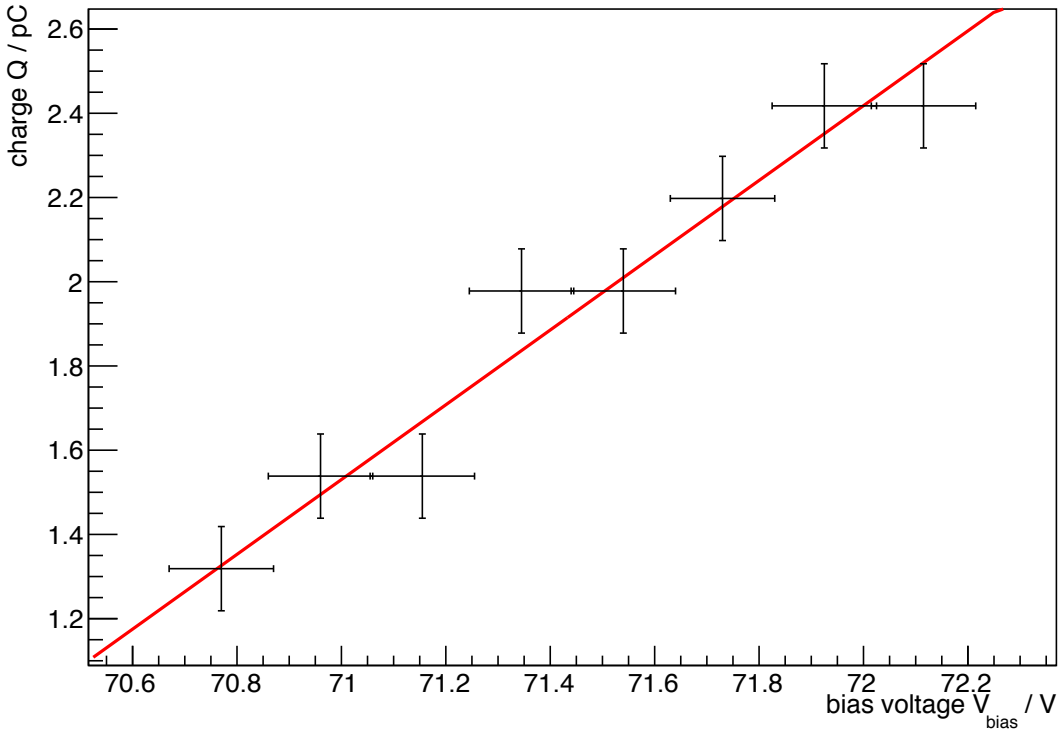

Figure 5.0.8: Breakdown-voltage calibration for SiPM no. 6.

Linear Regression for Mean QDC of Single Pixels

The fit results are shown in table 4.5.2.

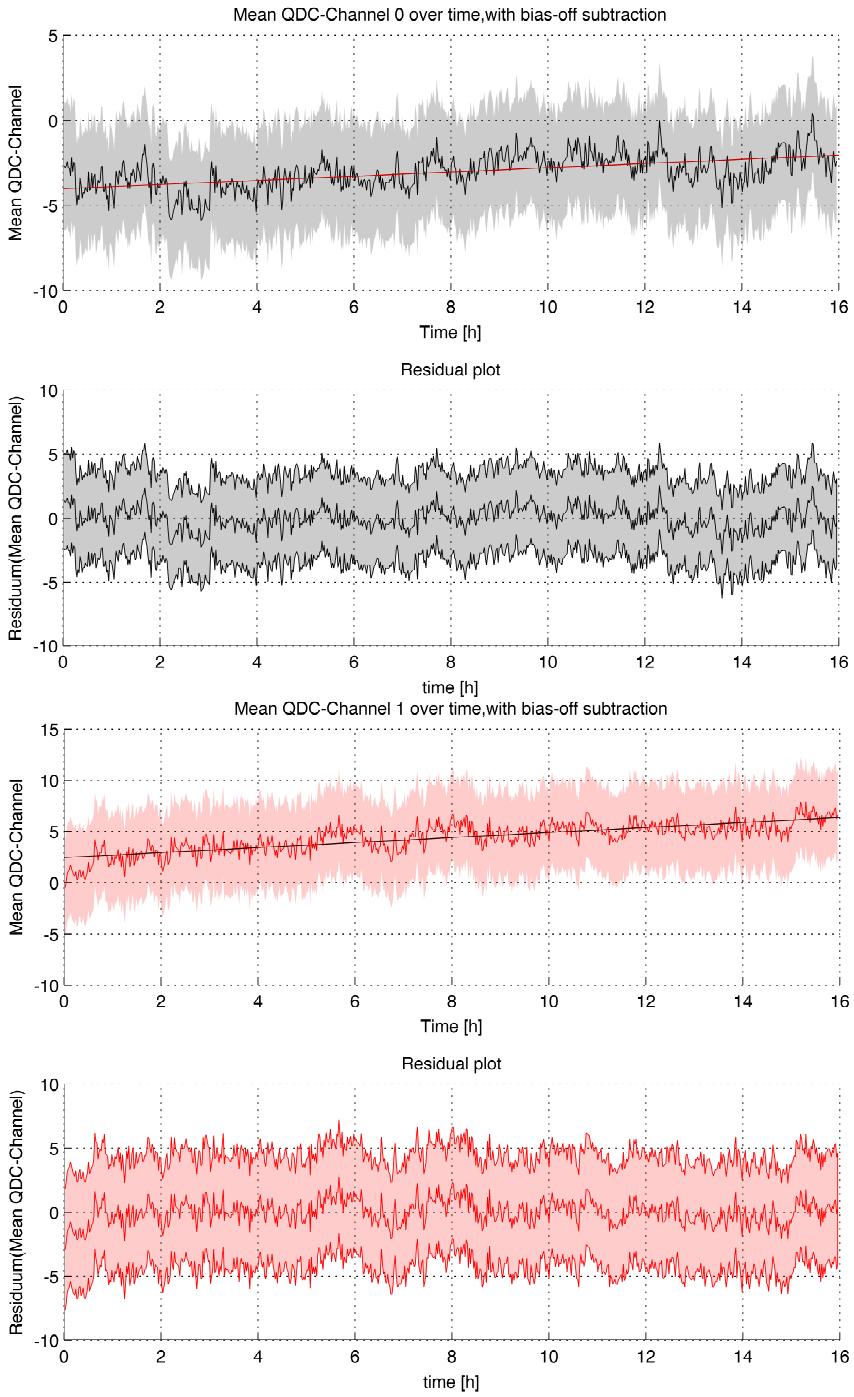

Figure 5.0.9: QDC mean time trace fit for SiPM no. 0 and 1 from top to bottom.

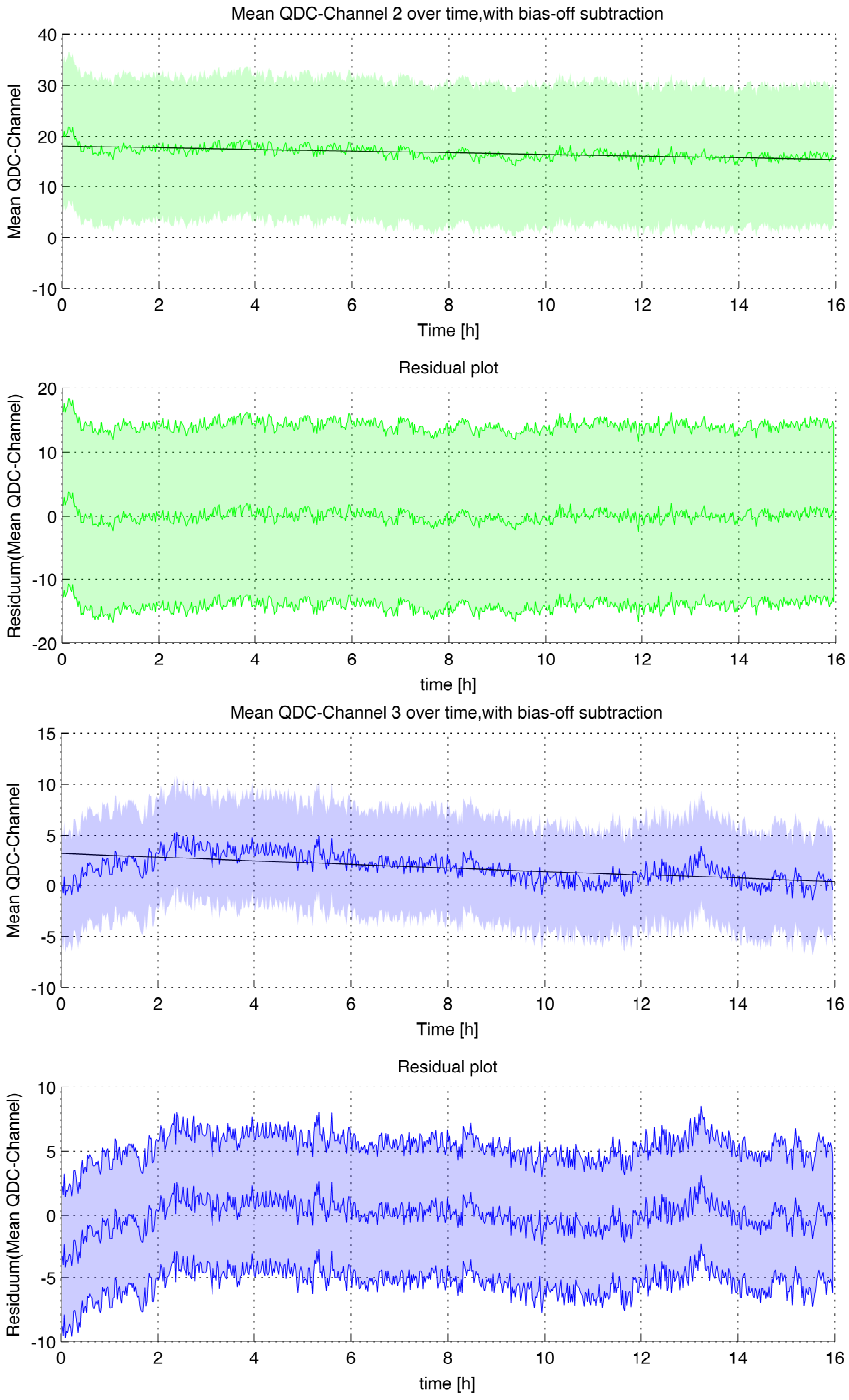

Figure 5.0.10: QDC mean time trace fit for SiPM no. 2 and 3 from top to bottom.

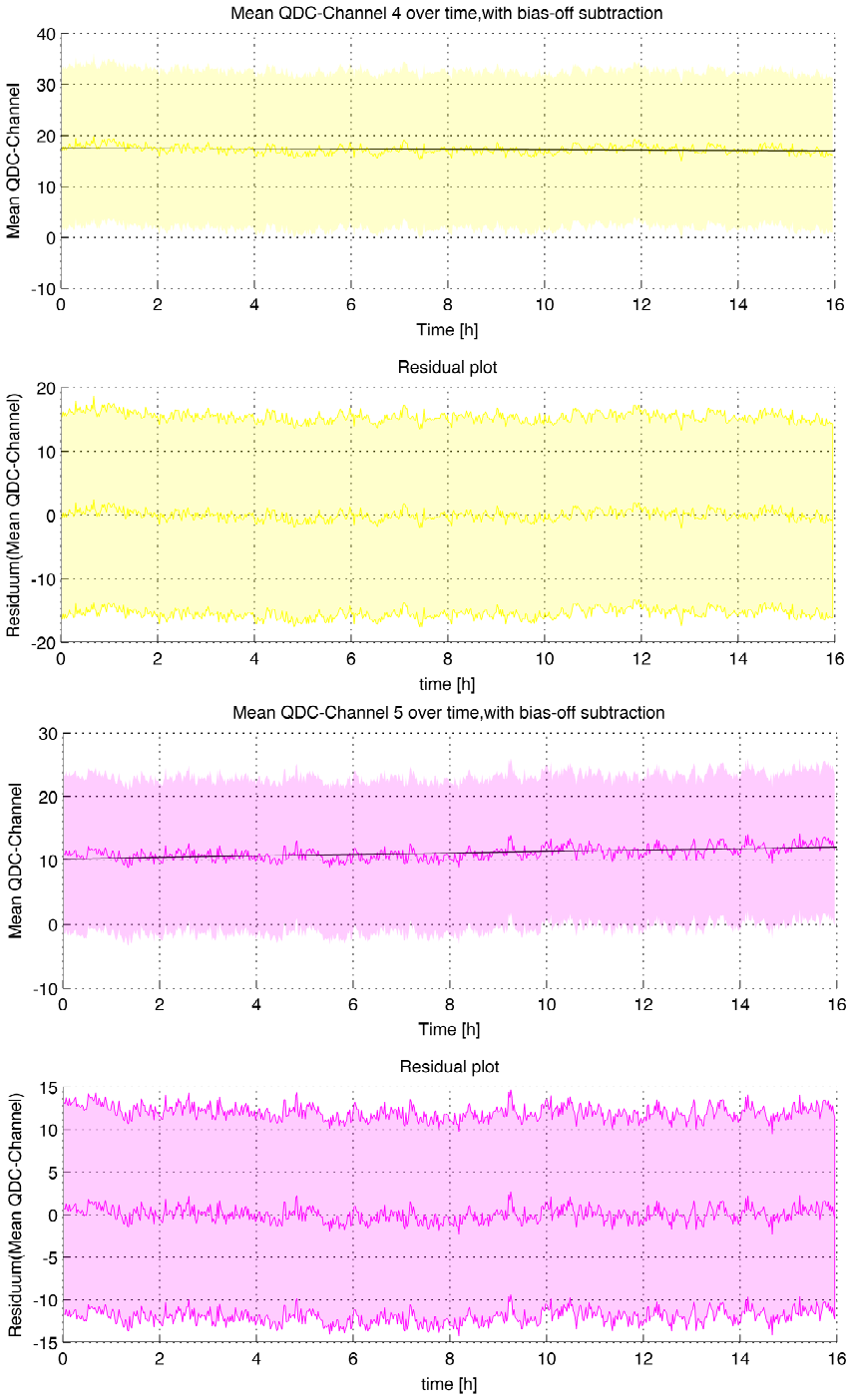

Figure 5.0.11: QDC mean time trace fit for SiPM no. 4 and 5 from top to bottom.

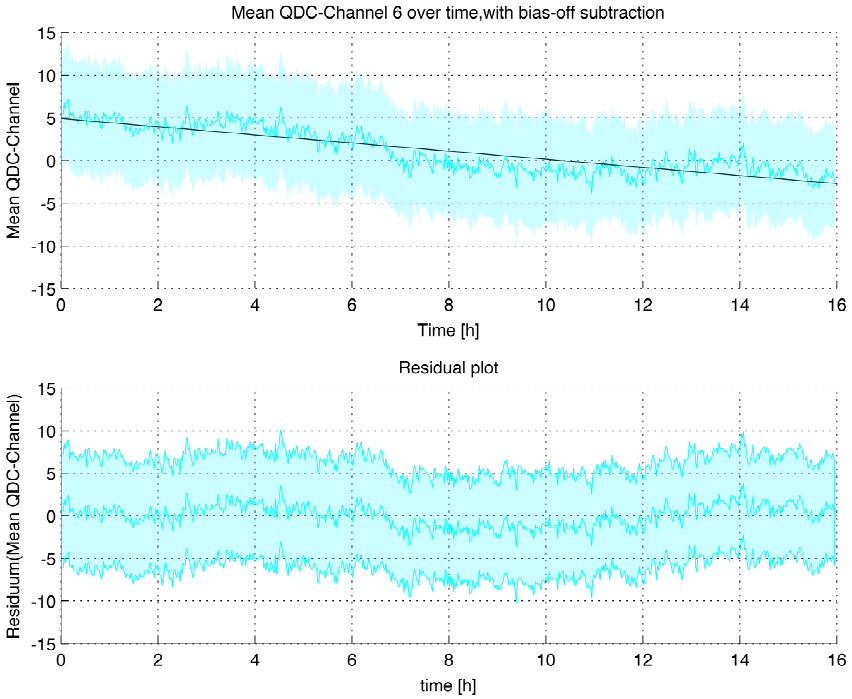

Figure 5.0.12: QDC mean time trace fit for SiPM no. 6.

Acknowledgements - Danksagungen

An dieser Stelle darf ich allen, die mich bei dieser Arbeit in den letzten 3 Monaten in jeglicher Form unterstützt haben, ganz herzlich danken.

Zunächst gilt mein Dank Herrn Prof. Dr. Hebbeker für das Ermöglichen dieser Arbeit als ein kleines eigenständiges Projekt. Am Rande bemerkt haben die gemeinsamen Meetings mir stets die Leidenschaft am wissenschaftlichen Arbeiten vermittelt. Des Weiteren geht ein Dank an Herrn Prof. Dr. Wiebusch für die Zweitkorrektur dieser Arbeit.

In erster Linie bin ich Tim Niggemann zu großem Dank verpflichted für die großartige Betreuung und für die Idee dieses Projekts. Herr Niggemann war immer offen für Fragen und Vorschläge und konnte mir bei jeglichen, vor allem programiertechnischen, Problemen weiterhelfen oder Alternativen aufzeigen. Vielen Dank auch für das Korrekturlesen der Arbeit. Darüber hinaus möchte ich noch allen Kollegen aus der Kollaboration um FAMOUS für die freundliche Aufnahme, die große Offenheit für Fragen und die angenehme Arbeitsatmosphäre danken.

Ganz besonders möchte ich dabei Lukas Middendorf für Unterstützung beim Löten und bei Fragen zu technischen Details, sowie Markus Lauscher für die Bereitstellung seiner Messinstrumente und der damit verbundenen Messzeit danken.

Insbesondere danke ich Herrn Barthel Phillips und den Mitarbeitern der Mechanik-Werkstatt des Instituts für die technischen Zeichnungen und die mechanische Konstruktion des Arduino Gehäuses.

Abschließend bedanke ich mich bei meiner Familie, meinen Freunden und ganz besonders bei meiner Freundin Celstina Trost für Begleitung und Unterstützung in dieser Zeit.

Erklärung

Hiermit versichere ich, dass ich diese Arbeit einschließlich beigefügter Zeichnungen, Darstellungen und Tabellen selbstständig angefertigt und keine anderen als die angegebenen Hilfsmittel und Quellen verwendet habe. Alle Stellen, die dem Wortlaut oder dem Sinn nach anderen Werken entnommen sind, habe ich in jedem einzelnen Fall unter genauer Angabe der Quelle deutlich als Entlehnung kenntlich gemacht.

Aachen, den 19. August 2013